NASA
Technical
Paper
1961

December 1981

# Thermal and Aerothermal Performance of a Titanium Multiwall Thermal Protection System

Don E. Avery,
John L. Shideler,
and Robert N. Stuckey




NASA

**NASA Technical Paper 1961**

1981

# Thermal and Aerothermal Performance of a Titanium Multiwall Thermal Protection System

Don E. Avery and
John L. Shideler
*Langley Research Center*
*Hampton, Virginia*

Robert N. Stuckey
*Lyndon B. Johnson Space Center*
*Houston, Texas*

NASA

Scientific and Technical
Information Branch

## SUMMARY

A metallic thermal protection system (TPS) concept called "multiwall" consists of discrete tiles which have multiple layers of dimpled and flat foil bonded together at the crest of the dimpled sheets. Titanium tiles designed for temperature and pressure at Shuttle body point 1140 where the maximum surface temperature is approximately 811 K have been tested to evaluate thermal performance and structural integrity.

A two-tile model of titanium multiwall and a model consisting of low-temperature reusable surface insulation (LRSI) tiles were exposed to 25 simulated thermal and pressure Shuttle entry missions in the Johnson Space Center Building 13 radiant heating system. The two models performed the same, and neither model deteriorated during the tests. Results of the tests indicate that redesign of the multiwall tiles could reduce tile thickness and or weight. Cumulative radiant heating time was approximately 20 hr.

A nine-tile model of titanium multiwall was subjected to seven radiant heating tests and eight radiant preheat aerothermal tests in the Langley 8-Foot High-Temperature Structures Tunnel. Wind-tunnel test conditions were at nominal Mach numbers of 5.6 and 6.5 with a total temperature between 1550 K and 1930 K and dynamic pressure between 23.2 and 25.6 kPa. Cumulative radiant heating time was approximately 6 hr and cumulative exposure time to the hypersonic stream was 294 s. The overall sound pressure level (OASPL) during the aerothermal tests was approximately 161 dB.

Tips on the multiwall tiles overhanging downstream tiles proved to be effective in preventing flow in the gaps between the tiles of the nine-tile model even though in some cases the tips buckled. The surface of the multiwall tiles also survived numerous small particle impacts from the tunnel stream.

Although numerous failures in the structural bonds occurred during the aerothermal test series, no catastrophic failures in the TPS structure occurred. These failures are attributed to improper constraint of thermal growth at the boundary of the array and to fabrication difficulties inherent in the initial tile design. Debonding did not occur on the center tile which had more realistic boundary conditions. Minor design changes should improve structural integrity without having an impact on the thermal protection ability of the titanium multiwall TPS.

These tests demonstrated the capability of a titanium multiwall thermal protection system to protect an aluminum surface during a Shuttle-type entry trajectory at locations on the vehicle where the maximum surface temperature is below 811 K.


## INTRODUCTION

A metallic tile thermal protection system (TPS) concept called "multiwall" is being studied at the Langley Research Center (refs. 1 to 4). An early version of the multiwall concept was studied for an internal liquid hydrogen tank for a reusable space transportation vehicle where the multiwall simultaneously performed the functions of TPS, primary structure, and tank (ref. 5). This concept consisted of alter

nate layers of dimpled and flat sheets welded at the crests of the dimpled sheets. Foil gage outer layers from which the air was evacuated served as thermal protection, and thicker inner layers formed a structural sandwich. The sandwich carried fuselage loads and served as tankage for cryogenic fuel. This design was unsuccessful because of high thermal stresses between the thermal protection layers and the structural layers and the inability of the outer layers to maintain the vacuum required to prevent cryopumping. However, results from this study led to the present multiwall concept which is a discrete tile, vented TPS. The redesign of the multiwall TPS to a discrete tile system alleviated the thermal stress problem. Each tile is supported near its corners, allowing for thermal bowing and expansion relative to the cooler primary structure to which the tile is mechanically attached. The tiles were designed for Shuttle body point 3140 (a location on the center line and slightly forward of the pilot's windshield). This location was chosen because the maximum surface temperature of 811 K is within the temperature capabilities of titanium.

Thermal performance of a two-tile model and, for comparison, a model of low-temperature reusable surface insulation (LRSI) (ref. 6) were evaluated by 25 radiant heating tests at the Johnson Space Center in the Building 13 radiant heating test system. The tests simulated temperature and pressure at body point 3140 for an orbiter entry mission. In addition to these tests, the aerothermal performance and structural integrity of an array of nine multiwall tiles was evaluated in the Langley 8-Foot High-Temperature Structures Tunnel (8' HTST). The model was subjected to seven radiant heating tests and eight radiant preheat/aerothermal tests. Most of the heating tests were representative of a Shuttle entry temperature history for body point 3140. For the aerothermal tests, radiant heaters were used to apply the first part of the entry temperature, and the 8' HTST provided aerothermal loading at the time of maximum surface temperature. The aerothermal tests were at local Mach numbers between 5.6 and 6.8, and the unit Reynolds number was approximately $1.9 \times 10^6$ per meter.

## SYMBOLS

| | |
|---|---|
| $M_\ell$ | local Mach number |
| $M_\infty$ | free-stream Mach number |
| $p$ | pressure, Pa |
| $q_\infty$ | free-stream dynamic pressure, kPa |
| $R$ | unit Reynolds number per meter |
| $t$ | time, s |
| $T$ | temperature, K |
| $T_{t,c}$ | total temperature in combustor, K |
| $T_{TS}$ | temperature on top surface, K |
| $x,y$ | coordinates of multiwall instrumentation, cm |
| $\alpha$ | angle of attack, deg |

## DESIGN AND FABRICATION OF MULTIWALL TILES

The design condition chosen to allow for the use of titanium 6Al-4V was a maximum surface temperature of 811 K. Additional design conditions were a maximum primary structure temperature of 450 K and a maximum differential pressure across the tile of 6.9 kPa. By using these design conditions, the titanium tile was designed for minimum weight. More detail is given in reference 1. Body point 3140 on the Space Shuttle satisfies these design conditions and was used as the design point. The location of this body point on the Shuttle orbiter is shown in figure 1. The temperature and pressure histories at this body point for Shuttle entry trajectory 14414.1C are shown in figure 2.

The multiwall tiles were sized based on the temperature and pressure conditions shown in figure 2. Current aerodynamic moldline constraints were not considered. The effective conductivity of the multiwall was calculated by using techniques published in reference 1. Even though the pressure is very low during most of the entry, it is greater than the threshold level of 0.0133 Pa below which the conductivity of air can be neglected. Consequently, air conductivity was included in calculating the effective conductivity of the multiwall. Free convection in the air volumes created by the dimpled and flat sheets was prevented by sizing the volumes such that the Grashof number was less than 2000 (ref. 1). The pitch and height of the dimpled sheets and the number of layers were determined so that the maximum temperature of a 0.41-cm-thick aluminum plate beneath the tile would not exceed 450 K.

Test tiles of this configuration were fabricated by Rohr Industries. Figure 3 shows an exploded view of a multiwall tile prior to fabrication by liquid interface diffusion (LID) bonding. (This bonding process, which requires significantly less contact pressure than conventional titanium diffusion bonding processes, is proprietary to Rohr Industries.) The dimpled sheets and edge closures were superplastically formed before bonding. One of the fabricated tiles with characteristic dimensions is shown in figure 4. The tile has a thickness of 1.75 cm and weights 3.66 kg per unit planform area ($m^2$). Details of the design and fabrication sequence are given in references 2 and 3. The edge closure for each tile is beaded to increase buckling strength and is skewed 25° relative to face sheets to provide a "scarfed" interface between adjacent tiles. These scarfed joints reduced heat transfer through the gaps between tiles by increasing conduction length and reducing the radiation view factor. A 0.51-cm-wide lip (fig. 4) overlaps adjacent and rear tiles downstream to reduce the possibility for flow in the gaps between tiles. A lower lip also extends under upstream tiles.

The attachment scheme is illustrated by the two-tile model shown in figure 5. Two attachment tabs are LID bonded to the tile underside on one edge. These attachment tabs slide under clips which are fastened to the aluminum plate which represents the vehicle primary structure. Each tab also slides through a clip which is bonded to the underside of an adjacent tile. Thus, each tab holds down a corner of two tiles. Shoulders on the tabs prevent excessive tile lateral motion, and the location of each tile is independently indexed on the structure. The perimeter of each tile rests on a strip of Du Pont Nomex felt 2.54 cm wide by 0.48 cm thick, which serves to inhibit any hot gas flow which might otherwise leak under the tile. Since the felt is compressed when the tile is attached, it provides a spring force and damping to prevent the tile from rattling.

## DESIGN AND FABRICATION OF MODELS

Two multiwall test models were fabricated: a two-tile model for cyclic radiant heating tests at the Johnson Space Center (JSC) and a nine-tile model (aerothermal model) for aerothermal tests in the Langley 8-Foot High-Temperature Structures Tunnel (8' HTST). A model consisting of the more widely known low-temperature reusable surface insulation (LRSI) tiles was also fabricated for testing at JSC to provide comparative data with the multiwall system. The top surface of the multiwall two-tile model and the nine-tile model was coated with a high-temperature paint (Sperex VHT SP-101). This coating provides a high solar reflectance for temperature control in orbit and a high emittance for entry heating. In addition, the tiles on these models were attached to an aluminum plate that represents the thermal mass of the primary structure at the design point.

### Cyclic Radiant Heating Models

The models for cyclic radiant heating tests (fig. 6) were a two-tile model of titanium multiwall and a model consisting of LRSI tiles of equal surface area. The two-tile model of titanium multiwall (figs. 5, 6(a), and 7) consisted of two tiles attached to an aluminum plate 34.87 by 73.03 by 0.41 cm. All the installation components (tabs, clips, and Nomex felt) intended for flight application were used. The coating on the two-tile model was inadvertently not cured before testing.

The LRSI model shown in figures 6(b) and 8 consisted of six 1.14-cm-thick LRSI tiles which were sized for the aerodynamic requirements at the design point. (The tile thickness at this body point on the Shuttle is greater than that required to protect the aluminum structure because it is sized to meet aerodynamic fairing requirements rather than thermal requirements alone.) Each tile was individually bonded with General Electric RTV 560 to a 0.41-cm-thick Nomex felt strain isolation pad (SIP) which was in turn bonded to an aluminum plate approximately the same size as that for the multiwall two-tile model. The SIP was sized 1.25 cm smaller than the LRSI on each edge to allow for Nomex felt strips (filler bars) 1.91 cm wide and 0.44 cm thick to be bonded to the primary structure around the perimeter on each SIP. (See fig. 6(b).) The LRSI TPS weighs 2.98 kg per unit planform area ($m^2$) at the design point.

### Aerothermal Model

The nine-tile model (fig. 9) used for aerothermal testing consisted of an array of nine multiwall tiles. In order to avoid long longitudinal gaps (a gap most nearly aligned with flow) between the multiwall tiles, the individual tiles were staggered and rotated 30° to the flow. The large wrinkles in the downstream corners were the result of tooling problems incurred during fabrication of the individual tiles. In order to expedite fabrication of the test articles the tools were not modified to eliminate the wrinkles. The aluminum plate representing the primary structure was supported by aluminum channels that were thermally isolated from the aluminum plate with Du Pont Teflon tape. The tile attachment clips on the aluminum plate and Nomex felt used to inhibit flow and rattling are shown in figure 10. These attachment schemes are the same intended for flight application. A low conductivity Glasrock material was installed around the tiles to provide a smooth aerodynamic surface and to thermally protect that part of the aluminum plate which was not covered by the tiles. Thermal expansion gaps were left between the multiwall tiles and the Glasrock and were filled with Harbison-Carborundum Fiberfrax felt insulation to prevent flow

into the gaps. This method of installation produced stiff edge conditions for the boundary tiles that partially restrained the tiles from thermal expansion. Although the edge condition is not representative of full-scale application, the edge conditions on the center tile where no Fiberfrax was used are considered to be realistic.

## APPARATUS AND PROCEDURE

### Cyclic Radiant Heating Tests

The multiwall two-tile model and the LRSI model (figs. 7 and 8) were mounted on a panel holder and exposed to 25 tests in the JSC Building 13 radiant heating test system. The tests simulated Shuttle entry temperature and pressure conditions shown in figure 2. Cumulative radiant heating time was approximately 20 hr.

Panel holder.- Each model was thermally isolated from an aluminum panel holder 121.92 by 121.92 cm by 0.64 cm thick by a 2.54-cm-thick layer of Lockheed LI-900 silica insulation placed between the panel holder and the aluminum plate representing the primary structure. The insulation was used to reduce heat losses from the backface of the primary structure. Additionally, each model was insulated around all sides level to the top surface (hot face) of the model with Fiberfrax insulation. A sketch of the LRSI model test configuration cross section is shown in figure 11. The multiwall model was installed in a similar manner.

Test facility.- The JSC Building 13 radiant heating test system (fig. 12) can simultaneously simulate the thermal (up to 1600 K) and pressure (down to 0.09 kPa) environments that spacecraft thermal protection systems are exposed to during ascent, orbit, and entry phases of a mission. The primary components of the system include a radiant heater system, a cryogenically cooled panel, a 11.33-$m^3$ vacuum test chamber, and a rain simulator.

The simulated ascent and entry heating environments are produced by a heater system consisting of electrically heated graphite elements enclosed in a gaseous nitrogen purged fixture box. One side of the heater system has a columbium susceptor plate to reradiate heat to the test model. The heater system is mounted in a boilerplate Apollo command-module test chamber (figs. 12 and 13) that is evacuated by a mechanical vacuum pump. The heater system and cryogenically cooled panel are mounted on rails to allow either one to be positioned over the test article during testing. Thus, the test model can be heated or cooled while vacuum conditions are maintained. Models up to 61 cm square can be tested in this facility. For the cyclic radiant heating tests, only the vacuum and radiant heater systems were used to simulate entry conditions.

Test procedure.- Both models were positioned within the test chamber with the top of each model about 2.54 cm below the heater. The heater was positioned over one of the test models, then the chamber was evacuated to less than 0.09 kPa. After the chamber pressure stabilized, the model was exposed to a simulated orbiter mission thermal and pressure entry test cycle. While the first model was cooling, the heater was positioned over the second model and the test sequence was repeated. The models were visually inspected after each cycle.

Instrumentation.- Instrumentation placement on the models was designed so that the performance of the multiwall model could be evaluated in response to cyclic radiant heating and so that comparisons could be made between the models. The multiwall two-tile model was instrumented with 26 No. 30 gage and 7 No. 24 gage chromel-alumel

thermocouples at the locations shown in figure 14. The dimensional locations are given in table I. The seven thermocouples on the back surface of the aluminum plate were attached by peening. All other thermocouples were sandwiched between the model and a titanium foil strap spot-welded to the model (fig. 15).

The thermocouple locations for the LRSI model are shown in figure 16. The eight thermocouples attached to the back of the aluminum plate were No. 24 gage chromel-alumel and were peened into the aluminum. The other seven thermocouples were No. 30 gage chromel-alumel and were either imbedded into the LRSI surface or sandwiched between LRSI and Nomex.

Data reduction.- Heater operating conditions, environmental test conditions, and model temperature response data were recorded by two data acquisition systems. One, an analog-to-digital recording system, digitizes analog data for all channels and records it on magnetic tape so that the data can be reduced at a later date to provide history plots. In addition, critical real-time data were recorded and displayed on the other system which consists of self-balancing potentiometer-type strip-chart recorders that also serve as a backup system for the analog-to-digital system.

## Aerothermal Tests

The nine-tile model was mounted in a panel holder and subjected to seven radiant heating tests and eight radiant preheat/aerothermal tests in the Langley 8' HTST. Four of the radiant heating tests were thermal cycles to cure the VHT SP-101 surface coating on the multiwall tiles. Except for the curing tests, all tests were representative of a typical Shuttle surface temperature history (fig. 2). A summary of all tests is given in table II. Also, wind-tunnel test conditions for the aerothermal portions of the tests are given in table III. Cumulative radiant heating time and aerothermal exposure time were approximately 6 hr and 294 s, respectively.

Panel holder.- The nine-tile model was installed in a panel holder (figs. 17 and 18) which can accommodate test models up to 108 by 152 cm. (See refs. 6 and 7.) The aluminum support channels of the model were bolted to I-beams spanning the panel holder model test area. The aerodynamic surface of the panel holder is covered with 2.54-cm-thick low-conductivity Glasrock tiles to thermally protect the internal structure. A sharp leading edge with a lateral row of spherical boundary-layer trips was used to promote a turbulent boundary layer whereas aerodynamic fences provide uniform two-dimensional flow over the entire aerodynamic surface. Surface pressure and aerodynamic heating rates were varied by pitching the panel holder to a predetermined angle of attack. Differential-pressure loading across the model was maintained at a minimum by venting the panel holder cavity to the lower pressure on the leeside of the panel holder through a series of check valves.

Test facility.- The 8' HTST (fig. 19) is a large blowdown facility that simulates aerodynamic heating and pressure loading at a nominal Mach number of 7 and at altitudes between 25 and 40 km. The high energy needed for this simulation is obtained by burning a mixture of methane and air under pressure in the combustor and expanding the products of combustion through a conical-contoured nozzle into the open jet test chamber. The flow enters a supersonic diffuser where an air ejector pumps the flow through a mixing tube and exhausts the flow to the atmosphere through a subsonic diffuser. This tunnel operates at combustor total temperatures between 1400 and 2000 K, free-stream dynamic pressure from 14 to 86 kPa, and free-stream unit Reynolds numbers per meter from $1.0 \times 10^6$ to $10.0 \times 10^6$.

The model is initially covered with a radiant heater system which also serves as an acoustic baffle and stored in a pod below the test stream (fig. 19(b)) to protect it from adverse tunnel start-up transients and acoustic loads. Once the desired flow conditions are established, the heater system is retracted and the model is rapidly inserted into the test stream (fig. 19(c)) on a hydraulically actuated elevator. A model pitch system provides an angle-of-attack range from -20° to 20°.

The radiant heating system can be used for the radiant heating tests and as a preheat for the aerothermal tests. The heater system consists of quartz-lamp radiators mounted beneath the acoustic baffles (fig. 19). The radiant heaters are powered by an ignitron power supply and are controlled by a closed-loop servo system to give the desired temperature histories. More detailed information about the 8' HTST can be found in references 7 and 8.

Test procedures.- Figure 20 shows a typical surface temperature history for a multiwall tile during the aerothermal tests. For the radiant heating tests, the aerothermal portion of the curve was omitted and the surface temperature followed the Shuttle trajectory until the required heating rate was below the value which the radiant heater system could control. For the radiant preheat/aerothermal tests, the surface was heated according to the entry trajectory temperature history (fig. 20) and was exposed to the wind-tunnel conditions at a preselected time within that temperature history. The procedure for the aerothermal part of the tests was to start the tunnel, obtain correct flow conditions, de-energize the radiant heaters, retract the heaters and acoustic baffles, and insert the model into the hypersonic stream while simultaneously pitching the panel holder. The time elapse between the heaters being de-energized and the model entering the stream was kept to a minimum (approximately 5 s). The desired angle of attack is reached prior to the model reaching the stream center line. The model was exposed to the hypersonic stream for as long as flow conditions could be maintained. At the end of the aerothermal exposure the procedure was reversed, and tunnel shutdown was initiated after the heaters and acoustic baffles had covered the model. Because of equipment problems, the radiant heaters could not be re-energized and natural cooling occurred. In these instances, the tiles were exposed to cooldown rates that were always more rapid than that shown in figure 20. The aerothermal tests were conducted at local nominal Mach numbers between 5.6 and 6.8, and the unit Reynolds number per meter was approximately $1.9 \times 10^6$ (table III).

Instrumentation.- Instrumentation placement on the multiwall nine-tile model was designed to evaluate the multiwall TPS design with reference to aerothermal loading. Instrumentation on the panel holder controlled the radiant heaters and measured the acoustic environment to which the nine-tile model was exposed. All model and tunnel instrumentation data were recorded by high-speed digital recorders.

The nine-tile model was instrumented with 52 No. 30 gage chromel-alumel thermocouples installed in the same manner as for the two-tile model. (See fig. 15.) Thermocouple locations can be determined from figure 21. In figure 21 the tiles are designated by a letter, and thermocouple locations for gap intersections are designated by a Roman numeral. Thermocouples were located on the tiles, in the tile gaps, and on the aluminum plate. Gap thermocouples were located at upstream and downstream terminals of longitudinal gaps.

The panel holder was instrumented with 10 thermocouples located on the Glasrock surface surrounding the model to monitor and control the radiant heater system. The panel holder was also instrumented with two water-cooled acoustic microphones to record the acoustic environment to which the model was exposed during test in the

8' HTST. An accelerometer was mounted close to each microphone to record the acceleration of the microphone so that the response of the microphones to acceleration could be separated from the acoustic response.

Data reduction.- During radiant heating tests and preheating prior to aerothermal exposure, thermocouple outputs were recorded at 2-s intervals. During the aerothermal portion of the tests, pressure and temperature data were recorded at 20 samples/s. Output from accelerometers and acoustic microphones were recorded on FM tape. All data were reduced to engineering quantities at the Langley Central Digital Data Recording Facility. Tunnel operating conditions reported herein for the wind-tunnel tests are based on the thermal, transport, and flow properties of the combustion products test medium as determined from reference 9. Free-stream conditions in the test section were determined from reference measurements in the combustion chamber by using results from tunnel-stream survey tests such as reported in reference 8. Local Mach number was obtained from oblique-shock relations.

## RESULTS AND DISCUSSION

### Cyclic Radiant Heating Tests

Structural performance.- The structural integrity of the two-tile multiwall model was maintained throughout the test series, although the coating began to flake at the beginning of the test series. It was learned after the test series began that the coating was uncured. The curing process removes the volatiles by slowly heating the coating to 756 K. Heating the model at the entry temperature rate shown in figure 2 was rapid enough to cause the coating to flake. The model condition before and after testing is shown in figures 7 and 22, respectively. Although the multiwall structure appeared to be undamaged after the 25 radiant heating tests, two areas were found where the face sheet debonded from the dimpled layer. The first area contained one debonded node and the other area contained approximately three debonded nodes. The model was not disassembled for close examination of the tile backface because further tests may be desired. The top surface lip of the front tile was properly in contact with the adjacent tile before testing started. However, after 25 thermal cycles, the lip was permanently deflected 0.10 cm above the adjacent tile surface. This deflection may result from a rotation of the tile edges caused by thermal bowing of the multiwall tiles. The bowing is spherical in nature because the temperature distribution through the thickness is approximately linear, and rotation occurs about the corner attachment points where the tile is essentially simply supported. The deflection is accentuated by the scarfed edge which locates the lip approximately 5.1 cm from the attachment. (See fig. 4.) The maximum edge deflection was hand calculated to be 0.35 cm. This calculated deflection would be lowered to 0.12 cm if the scarf angle were increased from 25° to 90°. Approximately 0.10 cm deflection can be accommodated before the yield stress is exceeded. Consequently, the permanent deformation could nearly be eliminated by use of a 90° edge closure and completely eliminated if a 0.02-cm vertical gap existed between the tile upper lip and the adjacent downstream tile.

Thermal performance.- The scarf joint between the two multiwall tiles forms a gap that may provide a path for heat flow. The temperature of the primary structure under the center of the multiwall tiles and beneath the gap between tiles (fig. 14) is shown in figure 23. The temperature directly under the gap (thermocouple 17) was very close to the temperatures beneath the center of the tiles (thermocouples 9

and 12). Thus, the thermal data indicate that no additional heat was transmitted down the gap. An analysis of the response of thermocouple 18, which was adjacent to the Nomex felt, indicates that thermocouple 18 was defective.

As previously mentioned, the multiwall tile thickness was determined for the temperature and pressure histories shown in figure 2, but the LRSI tile thickness was determined by an aerodynamic fairing requirement at body point 3140. Consequently, the LRSI tiles are thicker than would be required for thermal considerations only. Test data for the first test of the two models are shown in figure 24 along with the design and predicted temperature histories. Thermal performance was unchanged during the test series. Thus, these data are typical of each of the 25 cycles. The surface temperature histories (thermocouples 7 and 3) and the temperature histories of the aluminum plates (thermocouples 28 and 5) indicate that the thermal performance of the two systems was the same. Because the LRSI tile model is designed conservatively (thicker than that required for thermal design), it appears that the multiwall tile model is also designed conservatively.

The predicted aluminum plate response taken from reference 1 and shown in figure 24(a) is based on the design surface temperature history and assumes no heat loss from the aluminum plate. The measured thermal response (thermocouple 28) differs by as much as 86 K. The long-dash--short-dash curve shows the predicted temperature response using the measured surface temperature history (thermocouple 7) as the heat load and accounting for heat loss through 2.54 cm of LI-900 which was beneath the aluminum plate (fig. 11). This response is much closer to the measured response (thermocouple 28) but it is still as much as 29 K higher, which further substantiates that the analysis used for the thermal design of the multiwall is conservative.

## Aerothermal Tests

Structural performance.- Although numerous failures in the structural bonds occurred during the aerothermal test series, no catastrophic failure in the TPS structure occurred. Figures 25 and 26 show the condition of the multiwall nine-tile model surface before and after the aerothermal tests. A comparison of the two figures shows no significant difference in the surface condition. Surface debonding between the face sheet and the first dimpled sheet is shown in figure 27(a), and debonding between the backface and fourth dimpled sheet is shown in figure 27(b). Backface debonding was not discovered until after the test series was completed and the aerothermal model disassembled. A small amount of surface debonding was observed after the first radiant heating test (test 4). This debonding was concentrated in the corners of the tiles where fabrication difficulties were experienced. These difficulties were the results of inadequate dimple contact during bonding where the tile edge closure geometry would not allow tooling to react to the bonding loads. In order to prevent further damage from occurring, which might lead to a failure during aerothermal exposure, the debonded areas were repaired. The repairs were made by removing the VHT SP-101 coating from the damaged areas and repairing the bonds by spot-welding. The coating was then reapplied and cured. During the first aerothermal test (test 6), the tiles were exposed to an unrealistic thermal shock due to rapid cooling after the aerothermal exposure because equipment failure prevented the radiant heaters from being energized.

After test 6, many surface bonds were repaired on the tiles interfacing with the surrounding Glasrock. No repairs were required on the center tile. Most of the debonding occurred on tiles which were partially restrained from thermal growth by the surrounding Fiberfrax felt and Glasrock. These unrealistic boundary conditions

may have greatly contributed to the debonding. (These restraints did not exist on the two-tile model which was exposed to the cyclic radiant heating tests.) In addition to the occurrence of some surface debonding, a boundary tile lip at the trailing edge of the model was forced into the adjacent Glasrock (fig. 27(a)) and the lip on tile A buckled (fig. 28). The trailing edge overhanging the Glasrock was extended 0.51 cm over the Glasrock by spot-welding a 0.03-cm-thick titanium strip to the lip, and the buckled lip on tile A was repaired by reinforcing with a 0.03-cm-thick doubler 0.76 cm wide. Nevertheless, during test 7, additional buckling occurred on the lips of tile A (with the doubler) and tile B (without a doubler). The buckled lips were repaired by additional doublers (a second doubler on tile A). After these repairs, two radiant heating tests and six radiant preheat/aerothermal tests were made without further debonding or buckling of the lips.

At the conclusion of the test series, the aerothermal model was disassembled to examine the individual tiles. Figure 29(a) shows top surface cracks on tile A. The cracks occurred in the downstream corner of the tile where previously mentioned fabrication difficulties associated with the edge closures occurred. Additional damage occurred on the top surface where small particle penetrations were caused by rust particles in the wind-tunnel stream. Cracks in the lower surface lip and in the corrugated side walls of tile A are shown in figures 29(b) and (c). None of these problems resulted in TPS failure, and all this damage occurred in multiwall tiles which interfaced with the Glasrock as opposed to the center tile which interfaced solely with other multiwall tiles.

Minor design changes in the multiwall TPS have been identified to remedy the problems discussed above. The structural integrity should be improved significantly if the scarf angle relative to the face sheets is increased and if the node size of the dimple bond is increased. Buckling of the lips could be reduced by not staggering the alignment of the tiles so that thermal displacement of adjacent tiles are more compatible at the tile boundaries. Finally, use of the stronger Ti-6Al-2Sn-4Zr-2Mo alloy in place of Ti-6Al-4V alloy should help prevent permanent deformation of the lip. These changes would have a negligible impact on the thermal protection ability and mass of the multiwall TPS.

Thermal performance.- Typical thermal performance data for radiant heating tests and aerothermal tests on the nine-tile model are given by tests 9 and 15, respectively. The temperature histories measured through the center multiwall tile during a radiant heating test (fig. 30(a)) are nearly the same as that for the two-tile model previously discussed (fig. 24(a)). However, the surface temperature history for the nine-tile model is closer to the design (fig. 2); consequently, it was exposed to a higher heat load than the two-tile model. This higher heat load should have caused the temperature of the aluminum primary structure on the nine-tile model to be higher than that measured on the two-tile model. The fact that these temperatures are the same may be the result of the aluminum plate of the nine-tile model not being insulated on the backface to prevent heat losses to the cooler panel holder structure. Test 9 was intended to be a radiant preheat/aerothermal test; however, a tunnel malfunction prevented the model from being inserted into the stream. Consequently, the sudden reductions in temperature for thermocouples 43 and 38 which were caused by pressure transients during tunnel start-up (time approximately 800 s) should be ignored. During the aerothermal test (test 15), the maximum surface temperature was substantially higher (58 K) than the design temperature (fig. 30(b)). Because the heaters did not operate after the aerothermal exposure, the integrated heat load was less than the design heat load. Consequently, the maximum temperature of the aluminum plate is of little significance after aerothermal exposure. The expanded time scale shows the sequence of events that occur during an aerothermal

test. Again, the sudden reductions in temperature for thermocouples 43 and 38 are a result of tunnel start-up transients and model insertion into the tunnel flow. (See test procedure for aerothermal test.)

A major purpose of the aerothermal test was to determine if any flow occurred in the gaps between tiles and, hence, to determine if the lip joint and the Nomex strips under the perimeter of the tiles prevented heat flow to the primary structure. Several gap intersections were instrumented and temperature histories were recorded during radiant heating tests and aerothermal tests.

Temperature histories measured at an intersection near the point of the nine-tile model where a longitudinal gap terminates at a transverse gap are shown in figures 31(a) and (b) for tests 9 and 15, respectively. The temperature of the aluminum plate beneath the gaps was the same as the temperature beneath the center tile (thermocouple 51) for both the radiant heating test (fig. 31(a)) and the aerothermal test (fig. 31(b)). The temperatures recorded by thermocouples 2 and 3 are different even though both thermocouples 2 and 3 were located 0.64 cm below the top surface of tiles B and A, respectively. This temperature difference is caused by a slight difference in thermocouple locations: thermocouple 2 is located on tile B under the lips of both tile A and B, and thermocouple 3 is under the lip of tile A only.

Temperature histories measured at the same type of gap intersection located near the rear of the model (figs. 31(c) and (d)) show similar results except that nonuniform heating from the radiant heaters caused lower surface temperatures at the rear of the model but nonuniform aerothermal heating caused higher surface temperatures in this region. The differences in surface temperatures between the front and rear of the model during aerothermal heating may be a result of local flow disturbances caused by thermal bowing of the multiwall tiles, but instrumentation is insufficient to explain this phenomenon. Thermocouples 17 and 18 (expanded time scale in fig. 31(d)) show increasing gap temperatures during tunnel start-up. This temperature increase is much greater at this location than was measured at the front of the model (fig. 31(b)). Pressure differentials in the model during tunnel start-up are significantly higher than any flight condition. This start-up pressure differential apparently created very large flow rates of hot gases in the gaps; thereby, the temperatures of the gap walls were increased. The response during start-up indicates that the thermocouples would record any significant flow through the gaps during aerothermal exposure. Since trends established during radiant heating are the same during aerothermal exposure after start-up conditions ceased, it appears that the lip prevents flow ingress for pressure differences induced by skin friction.

If aerodynamic flow were to occur in a gap, the heating due to that flow would be expected to be less severe where a longitudinal gap originates at a transverse gap than where it terminates at a transverse gap. Temperature histories at the origin of a gap are shown in figure 32 for tests 9 and 15. As would be expected, these temperatures are lower than those shown in figure 31. However, the origin of the gap (fig. 32) is located in a relative cool region near the boundary between banks of radiant heaters, and thermocouples 46 and 49 (fig. 32(b)) are located in a slightly cooler position than thermocouples 2 and 3 (fig. 31(b)). Thus, the lower temperatures shown in figure 32 do not conclusively determine the existence or absence of heating in the gap.

A comparison of the maximum temperatures at the more severe type of gap intersection measured during radiant heating and measured during aerothermal heating (fig. 33) indicate the absence of any significant heating due to aerodynamic flow. The maximum temperatures measured at three depths in the gap are nondimensionalized

by the average top surface temperature. Data are compared for the typical radiant heating test (test 9) and the radiant preheat/aerothermal test (test 15) previously discussed. The very small difference between temperature ratios for the two types of tests indicates that the hot boundary-layer gases do not penetrate into the thermal expansion gaps of the multiwall TPS (except perhaps during tunnel start-up transients as previously discussed). Other locations and tests show the same results.

Acoustic environment.- The Shuttle trajectory will expose a TPS to an acoustic environment that has the potential of causing structural damage to lightweight systems. The acoustic environment in the test stream generated by the 8' HTST was recorded to determine the acoustic environment to which the nine-tile model was exposed during testing. The 1/3-octave-band acoustic spectrum for a representative test (test 14), is shown in figure 34. The overall sound pressure level (OASPL) was 163 dB. Acoustic data at body point 3140 for the Space Shuttle for lift-off conditions and for the design limit trajectory are shown for comparison. The figure shows that the acoustic environment during the aerothermal tests was approximately the same as the Shuttle design limit trajectory. This acoustic environment may have contributed to the previously discussed debonding of the tile face sheet. However, the center tile, which had realistic boundary conditions and which required no bonding repairs, was not damaged by this environment.

## CONCLUDING REMARKS

Titanium multiwall thermal protection system (TPS) tiles designed for Shuttle body point 3140 where the maximum surface temperature is approximatley 811 K have been tested to evaluate thermal performance and structural integrity. These multiwall tiles have a thickness of 1.75 cm and a mass per unit planform area of 3.66 $kg/m^2$. A model consisting of low-temperature reusable surface insulation (LRSI) tiles having a mass per unit planform area of 2.98 $kg/m^2$ designed to meet an aerodynamic fairing requirement and a two-tile multiwall model thermally designed for the same body point were subjected to 25 radiant heating tests in the Johnson Space Center Building 13 radiant heating system. The tests simulated temperatures and pressures for an orbiter entry mission at body point 3140. Cumulative radiant heating time was approximately 20 hr. A nine-tile model designed for the same body point was subjected to seven radiant heating tests and eight radiant preheat/aerothermal tests in the Langley 8-Foot High-Temperature Structures Tunnel. Wind-tunnel test conditions were at nominal Mach numbers between 5.6 and 6.8 with a total temperature between 1550 and 1930 K and a dynamic pressure between 23.2 and 25.6 kPa. Cumulative radiant heating time on the nine-tile model was approximately 6 hr and total exposure time to the hypersonic stream was 294 s.

Comparison of the thermal performance of the multiwall two-tile model with the thermal performance of the LRSI model showed that the maximum temperatures of the aluminum plate representative of the Shuttle primary structure under each of the TPS were the same. The ability of both models to protect an aluminum plate did not deteriorate after 25 thermal exposures, and the test results indicate that the multiwall thermal design is conservative. Also, the structural integrity of both models was maintained throughout the test series except for a small number of failures in the structural bonds of the two-tile multiwall model.

Although numerous failures in the structural bonds of the nine-tile multiwall model occurred during the aerothermal test series, no catastrophic failures in the TPS structure occurred. Most of the debonding occurred on tiles with boundary conditions which were partially restrained from thermal growth, a condition more severe

than was used to design the tiles. The center tile of the nine-tile model had realistic boundary conditions and experienced a negligible amount of debonding. An unrealistic thermal shock at the end of each aerothermal test may have contributed to the debonding problem. Some bonds were repaired by spot-welding; however, once a strong bond was obtained, two radiant heating tests and six radiant preheat/aerothermal tests were made without any further repair. The surface of the multiwall tiles also survived numerous small particle impacts from the tunnel stream. The lips on the multiwall tiles proved to be effective in preventing flow in the gaps between the tiles of the nine-tile model even though in some cases the lips buckled. During each aerothermal exposure the multiwall model was exposed to an overall sound pressure level of approximately 163 dB.

The geometry of the tiles presented fabrication difficulties which may have contributed to the debonding problems; however, minor design changes should improve the structural integrity without having a significant impact on the thermal protection ability or mass of the titanium multiwall TPS. These design changes include (1) increasing the scarf angle relative to the face sheets, (2) not staggering the alignment of the tiles, (3) increasing the dimple node size, and (4) changing material to the stronger Ti-6Al-2Sn-4Zr-2Mo alloy.

These tests demonstrate the capability of a titanium multiwall thermal protection system to protect a surface where the maximum temperature is below 811 K; thus, the multiwall is a viable alternate thermal protection system for Shuttle LRSI and advanced space transportation systems.

Langley Research Center
National Aeronautics and Space Administration
Hampton, VA 23665
November 25, 1981

## REFERENCES


1. Jackson, L. Robert; and Dixon, Sidney C.: A Design Assessment of Multiwall, Metallic Stand-Off, and RSI Reusable Thermal Protection Systems Including Space Shuttle Application. NASA TM-81780, 1980.

2. Blair, Winford; Meaney, John E., Jr.; and Rosenthal, Herman A.: Design and Fabrication of Titanium Multi-Wall Thermal Protection System (TPS) Test Panels. NASA CR-159241, 1980.

3. Blair, W.; Meaney, J. E.; and Rosenthal, H. A.: Fabrication of Titanium Multi-Wall Thermal Protection System (TPS) Test Panel Arrays. NASA CR-159383, 1980.

4. Shideler, John L.; Kelly, H. Neale; Avery, Don E.; Blosser, Max L.; and Adelman, Howard M.: Multiwall TPS - An Emerging Concept. NASA TM-83133, 1981.

5. Jackson, L. Robert; Davis, John G., Jr.; and Wichorek, Gregory R.: Structural Concepts for Hydrogen-Fueled Hypersonic Airplanes. NASA TN D-3162, 1966.

6. Emde, Wendall D.: Thermal Protection System for the Shuttle Orbiter. Bicentennial of Materials Progress, Volume 21 of National SAMPE Symposium and Exhibition, Soc. Advance. Mater. & Process. Eng., 1976, pp. 964-978.

7. Deveikis, William D.; Bruce, Walter E., Jr.; and Karns, John R.: Techniques for Aerothermal Tests of Large, Flightweight Thermal Protection Panels in a Mach 7 Wind Tunnel. NASA TM X-71983, 1974.

8. Deveikis, William D.; and Hunt, L. Roane: Loading and Heating of a Large Flat Plate at Mach 7 in the Langley 8-Foot High-Temperature Structures Tunnel. NASA TN D-7275, 1973.

9. Leyhe, E. W.; and Howell, R. R.: Calculation Procedure for Thermodynamic, Transport, and Flow Properties of the Combustion Products of a Hydrocarbon Fuel Mixture Burned in Air With Results for Ethylene-Air and Methane-Air Mixtures. NASA TN D-914, 1962.

TABLE I.- LOCATIONS OF THERMOCOUPLES ON MULTIWALL TWO-TILE MODEL

| Thermocouple (a) | x, cm | Y, cm | Depth location |
|---|---|---|---|
| 1 | 30.18 | 60.96 | Top surface of multiwall tile |
| 2 | 30.18 | 60.96 | Backside of multiwall tile |
| 3 | 29.79 | 29.85 | Top surface of multiwall tile |
| 4 | 29.79 | 29.85 | Backside of multiwall tile |
| 5 | 29.79 | 5.08 | Top surface of multiwall tile |
| 6 | 29.79 | 4.83 | Backside of multiwall tile |
| 7 | 17.78 | 47.50 | Top surface of multiwall tile |
| 8 | 17.78 | 47.50 | Backside of multiwall tile |
| 9 | 17.78 | 47.50 | Top surface of primary structure |
| 10 | 17.78 | 17.78 | Top surface of multiwall tile |
| 11 | 17.78 | 17.78 | Backside of multiwall tile |
| 12 | 17.78 | 17.78 | Top surface of primary structure |
| 13 | 19.05 | 33.96 | 0.64 cm below top surface |
| 14 | 19.05 | 34.80 | 0.64 cm below top surface |
| 15 | 17.78 | 32.26 | Midpoint of slope |
| 16 | 14.48 | 33.96 | 0.64 cm above backside of multiwall tile |
| 17 | 14.48 | 33.96 | Top surface of primary structure |
| 18 | 14.48 | 36.07 | Top surface of primary structure |
| 19 | 17.78 | 60.20 | Top surface of multiwall tile |
| 20 | 17.78 | 5.08 | Top surface of multiwall tile |
| 21 | 4.32 | 29.97 | Top surface of multiwall tile |
| 22 | 4.83 | 29.97 | Backside of multiwall tile |
| 23 | 5.08 | 59.69 | Top surface of multiwall tile |
| 24 | 5.08 | 5.08 | Top surface of multiwall tile |
| 25 | 17.02 | 33.53 | Midpoint of slope |
| 26 | 14.22 | 34.80 | 0.64 cm above backside of multiwall tile |
| 27 | 17.78 | 17.78 | 0.64 cm above backside of multiwall tile |
| 28 | 17.78 | 47.50 | Backside of primary structure |
| 29 | 30.18 | 60.96 | Backside of primary structure |
| 30 | 29.79 | 4.83 | Backside of primary structure |
| 31 | 5.08 | 5.08 | Backside of primary structure |
| 32 | 5.08 | 59.69 | Backside of primary structure |
| 33 | 14.48 | 33.96 | Backside of primary structure |

[a]See figure 14.

TABLE II.- SUMMARY OF TESTS FOR NINE-TILE MODEL

| Test | Type of test | Maximum radiant $T_{TS}$ (AV), K | Maximum aerothermal $T_{TS}$ (AV), K | Time, s | |
|---|---|---|---|---|---|
| | | | | Radiant | Aerothermal |
| 1 | Coating cure | 585 | | 3018 | |
| 2 | Coating cure | 615 | | 1350 | |
| 3 | Coating cure | 795 | | 1800 | |
| 4 | Radiant | 797 | | 1800 | |
| 5 | Coating cure | 777 | | 4600 | |
| [a]6 | Aerothermal | 798 | No data | 1083 | 42 |
| 7 | Aerothermal | 807 | 874 | 1100 | 25 |
| 8 | Aerothermal | 801 | 877 | 744 | 31 |
| 9 | Radiant | 811 | | 1400 | |
| 10 | Aerothermal | 811 | 874 | 746 | 29 |
| 11 | Aerothermal | 813 | 874 | 729 | 21 |
| 12 | Aerothermal | 812 | 875 | 781 | 44 |
| 13 | Radiant | 810 | | 725 | |
| 14 | Aerothermal | 803 | 865 | 724 | 51 |
| 15 | Aerothermal | 817 | 872 | 724 | 51 |

[a]No recorded data; all test conditions are approximate.

TABLE III.- WIND-TUNNEL TEST CONDITIONS FOR AEROTHERMAL TESTS

| Test | $T_{t,c}$, K | $M_\infty$ | $M_\ell$ | $q_\infty$, kPa | R | $\alpha$, deg |
|---|---|---|---|---|---|---|
| [a]6 | | | | | | 0 |
| 7 | Instrumentation saturated | | | | | 6.0 |
| [b]8 | 1550<br>1920 | 6.29<br>7.07 | 5.6 | 23.2<br>25.6 | $2.01 \times 10^6$<br>$1.84 \times 10^6$ | 5.0 |
| 10 | 1830 | 6.91 | 5.6 | 24.4 | $1.87 \times 10^6$ | 5.0 |
| 11 | 1850 | 6.94 | 5.6 | 24.8 | $1.87 \times 10^6$ | 5.0 |
| 12 | 1820 | 6.90 | 6.4 | 24.2 | $1.90 \times 10^6$ | 2.9 |
| 14 | 1830 | 6.91 | 6.5 | 24.3 | $1.86 \times 10^6$ | 2.9 |
| 15 | 1930 | 7.09 | 6.8 | 25.3 | $1.81 \times 10^6$ | 2.9 |

[a]No recorded data; all test conditions are approximate.
[b]Tunnel test conditions changed during aerothermal exposure.

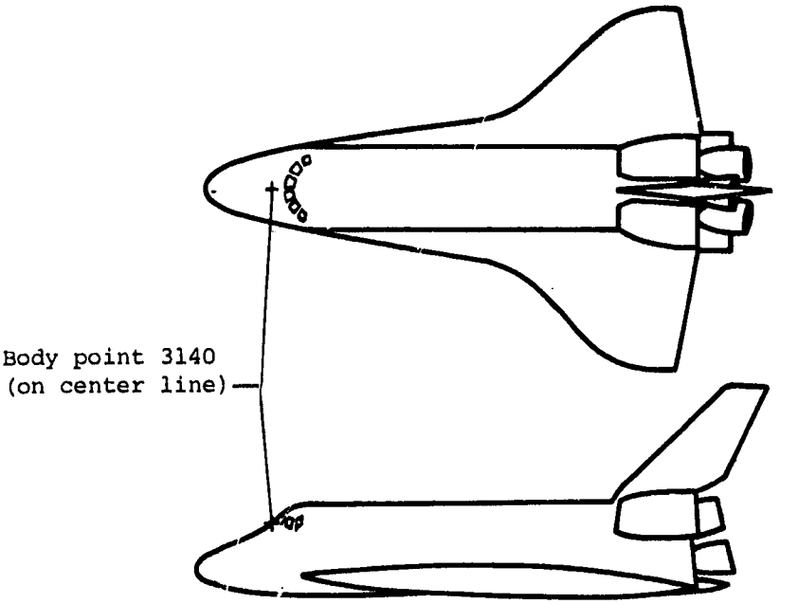


Figure 1.- Location of body point 3140 on Space Shuttle.

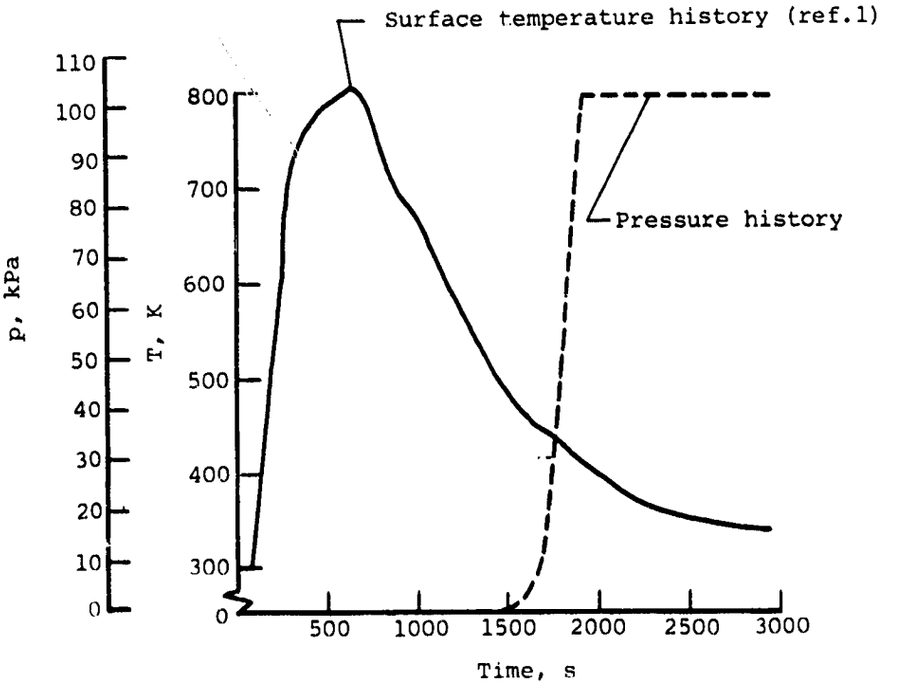


Figure 2.- Shuttle surface temperature and pressure history at body point 3140 Shuttle entry trajectory 14414.1C.

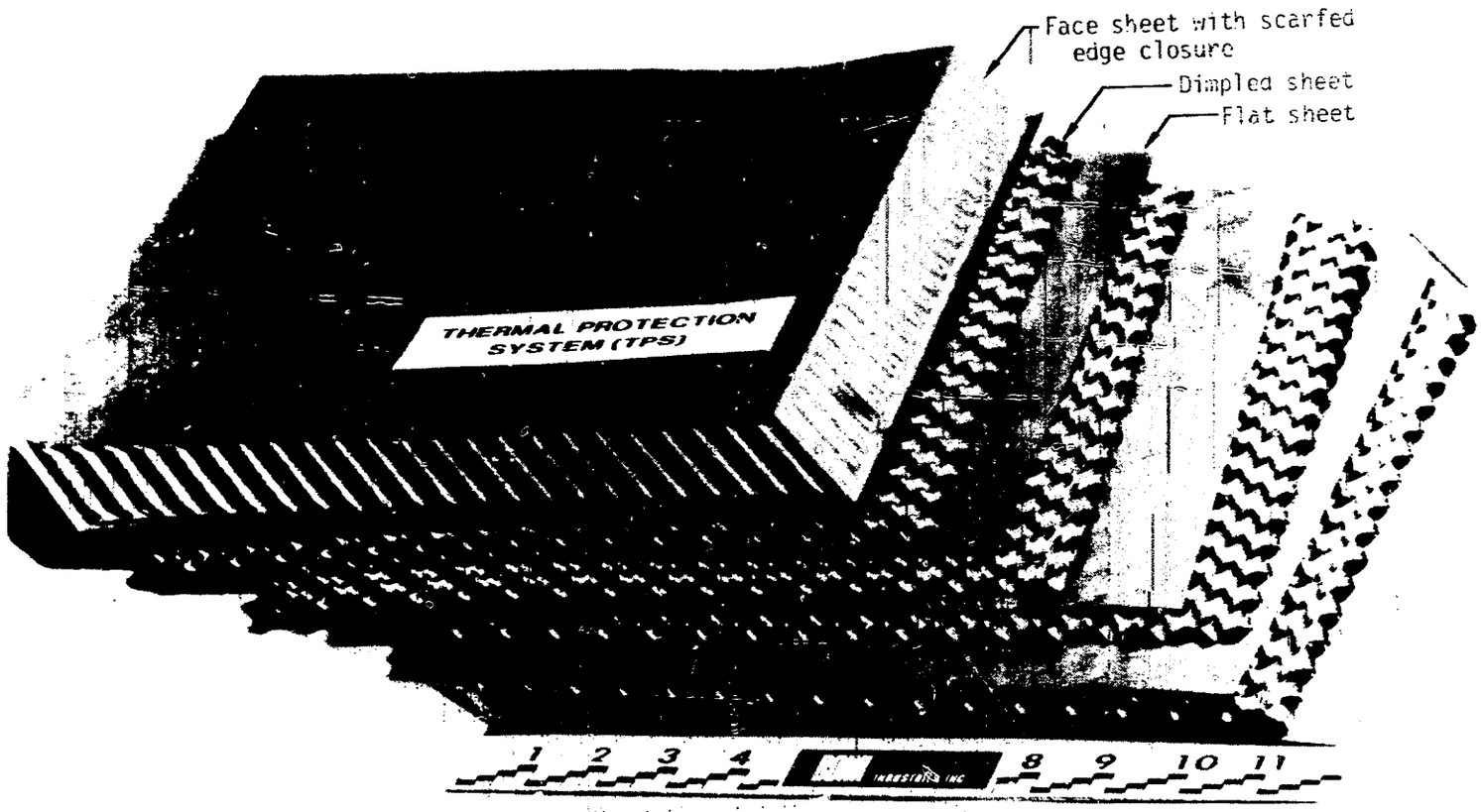


L-81-238

Figure 3.- Exploded view of titanium multiwall tile (scale in inches).

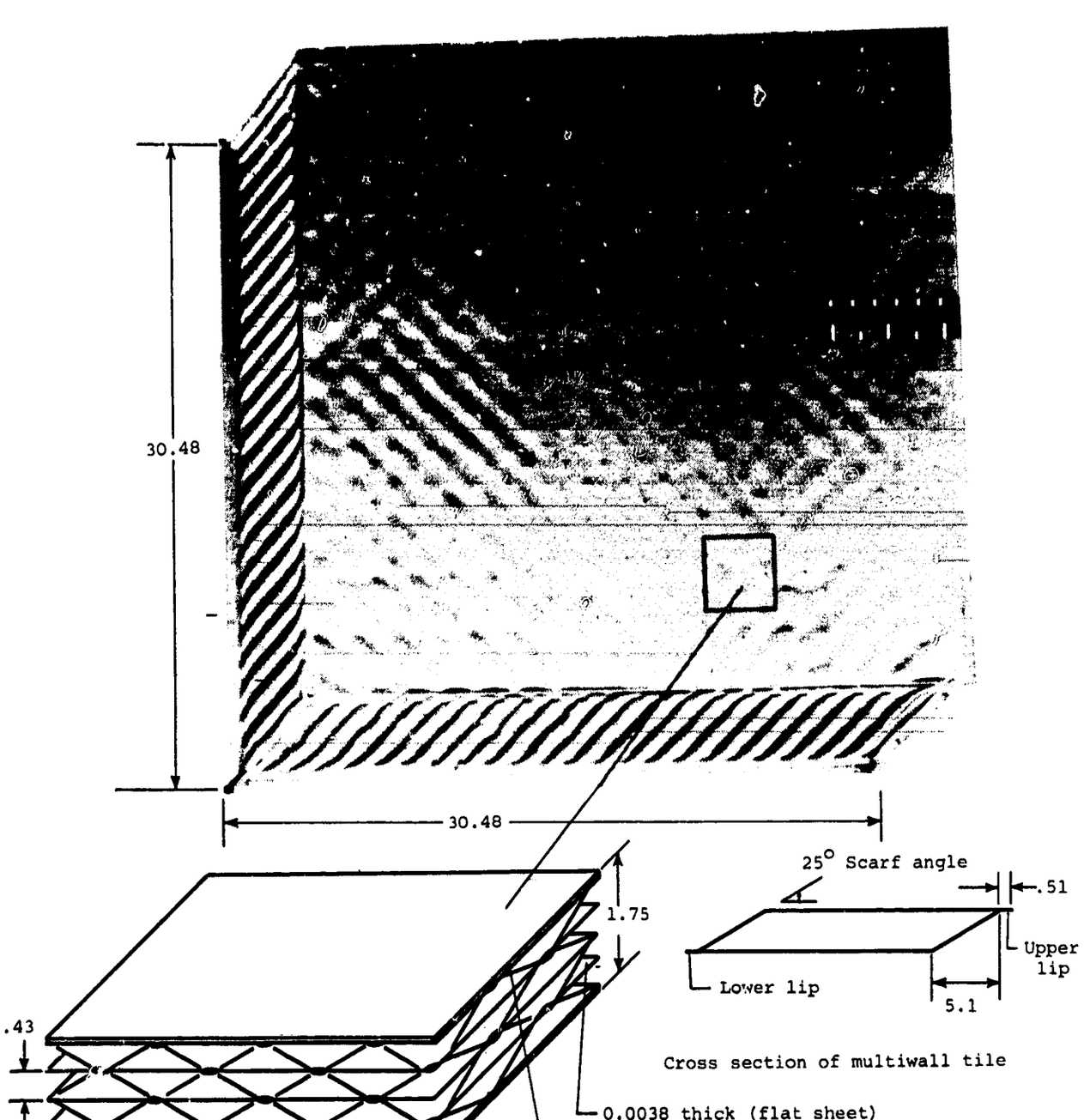


Figure 4.- Assembled multiwall tile. Dimensions are in centimeters.

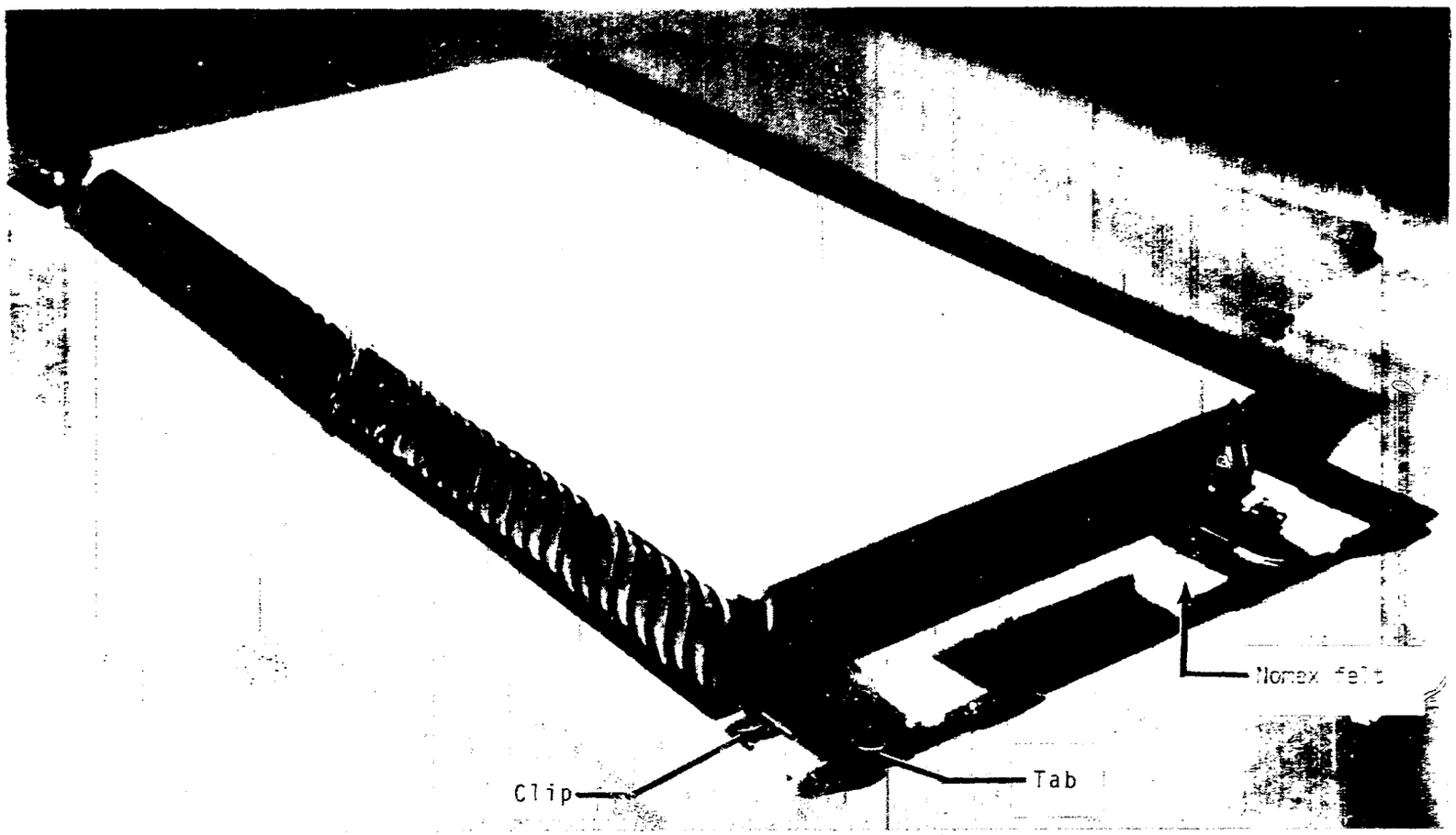


Figure 5.- Two-tile model of multiwall TPS.

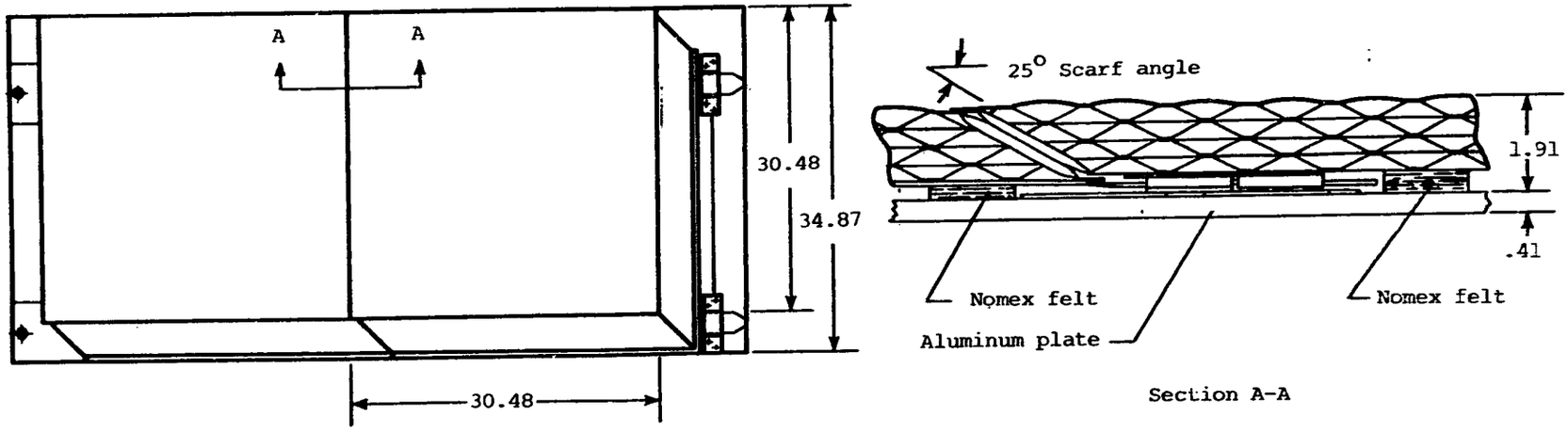


(a) Multiwall two-tile model.

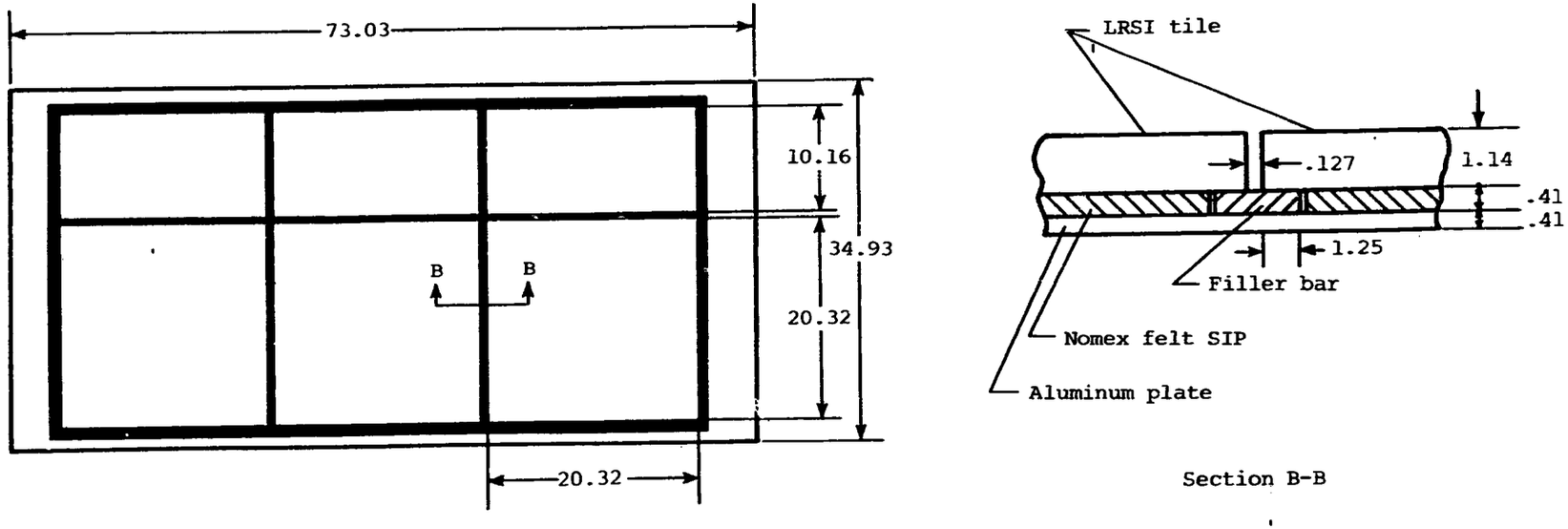


(b) LRSI model.

Figure 6.- Radiant cyclic heating models. Dimensions are in centimeters.

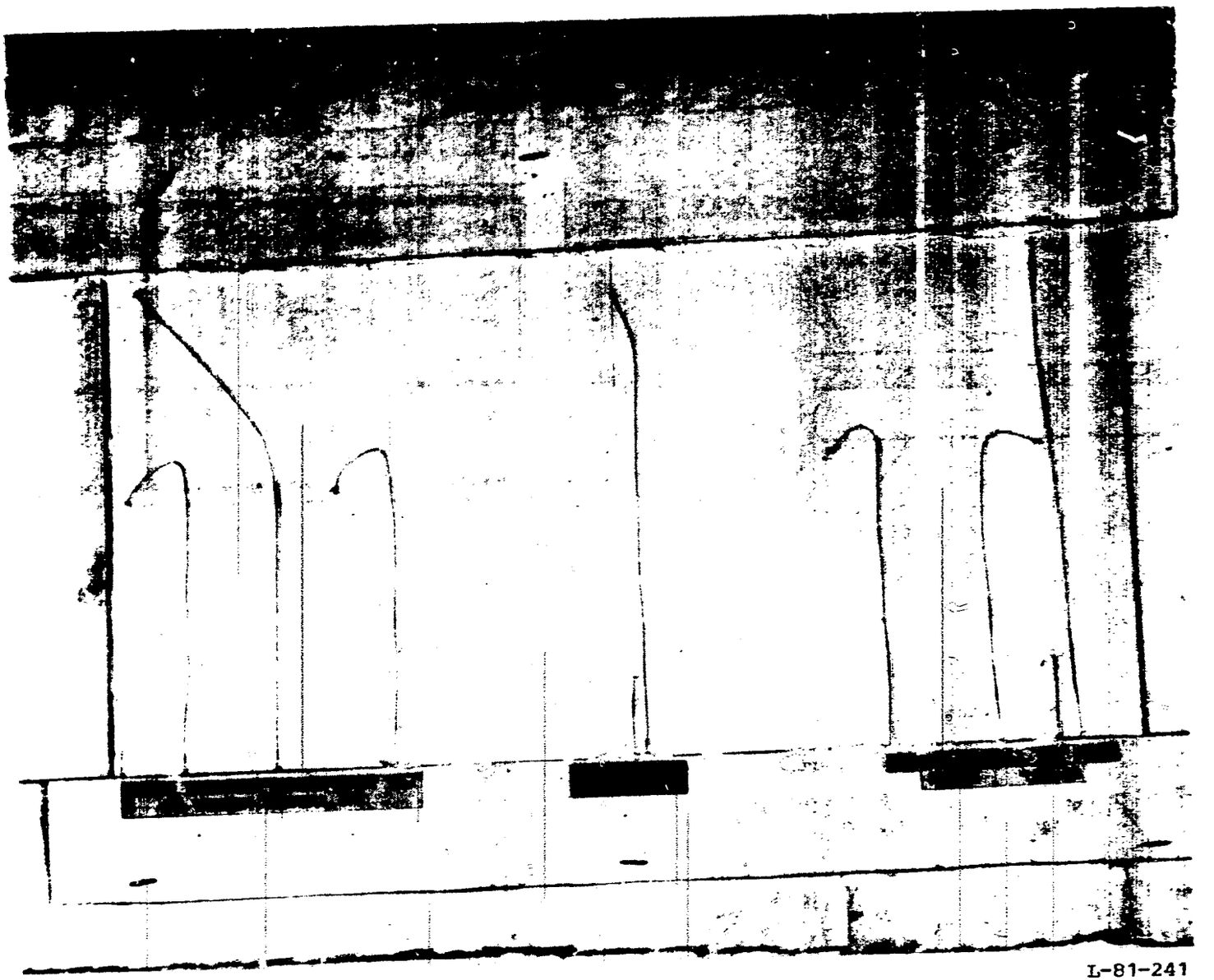


Figure 7.- Two-tile model of multiwall TPS installed in panel holder before testing.

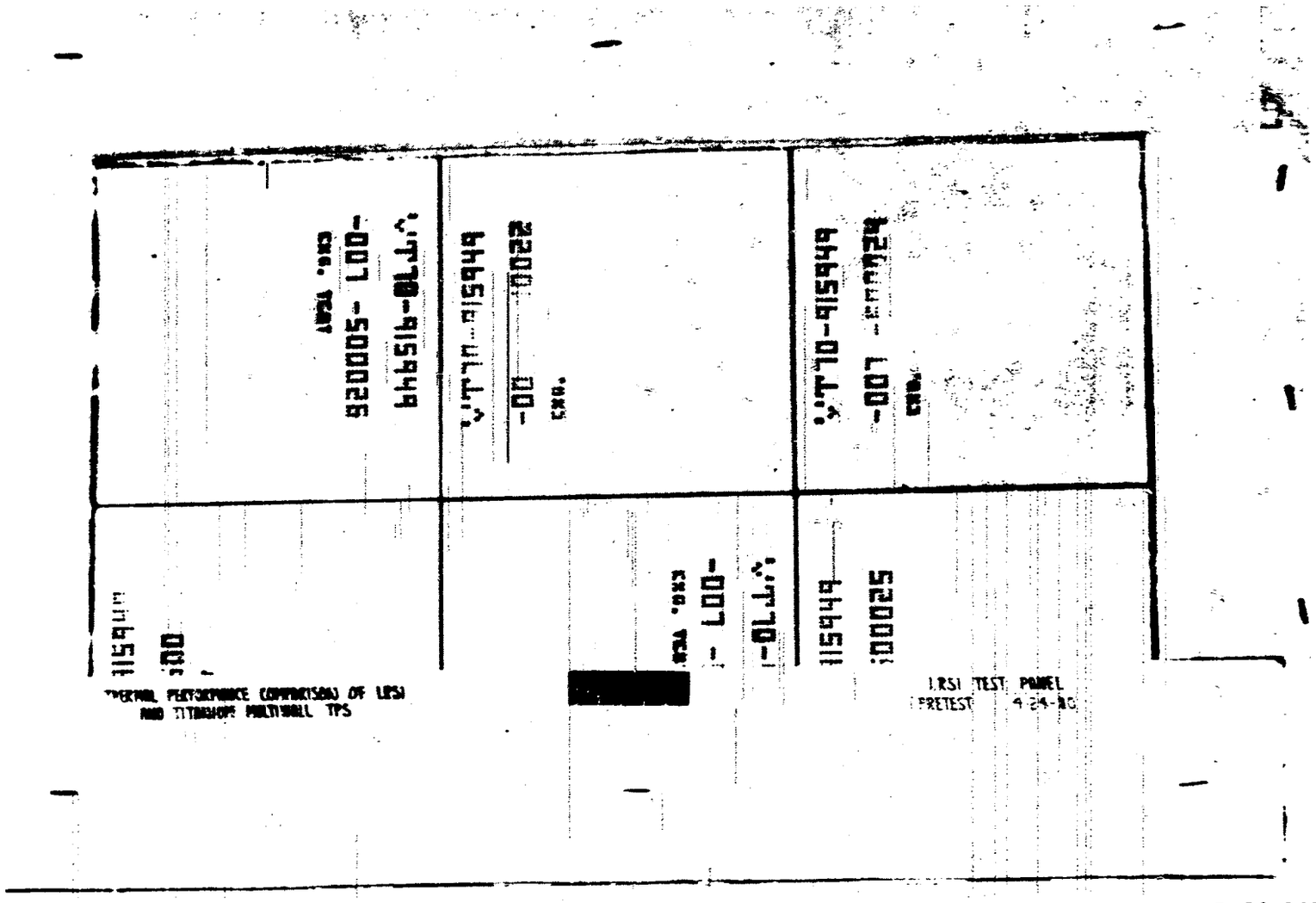


L-81-242

Figure 8.- LRSI model before testing.

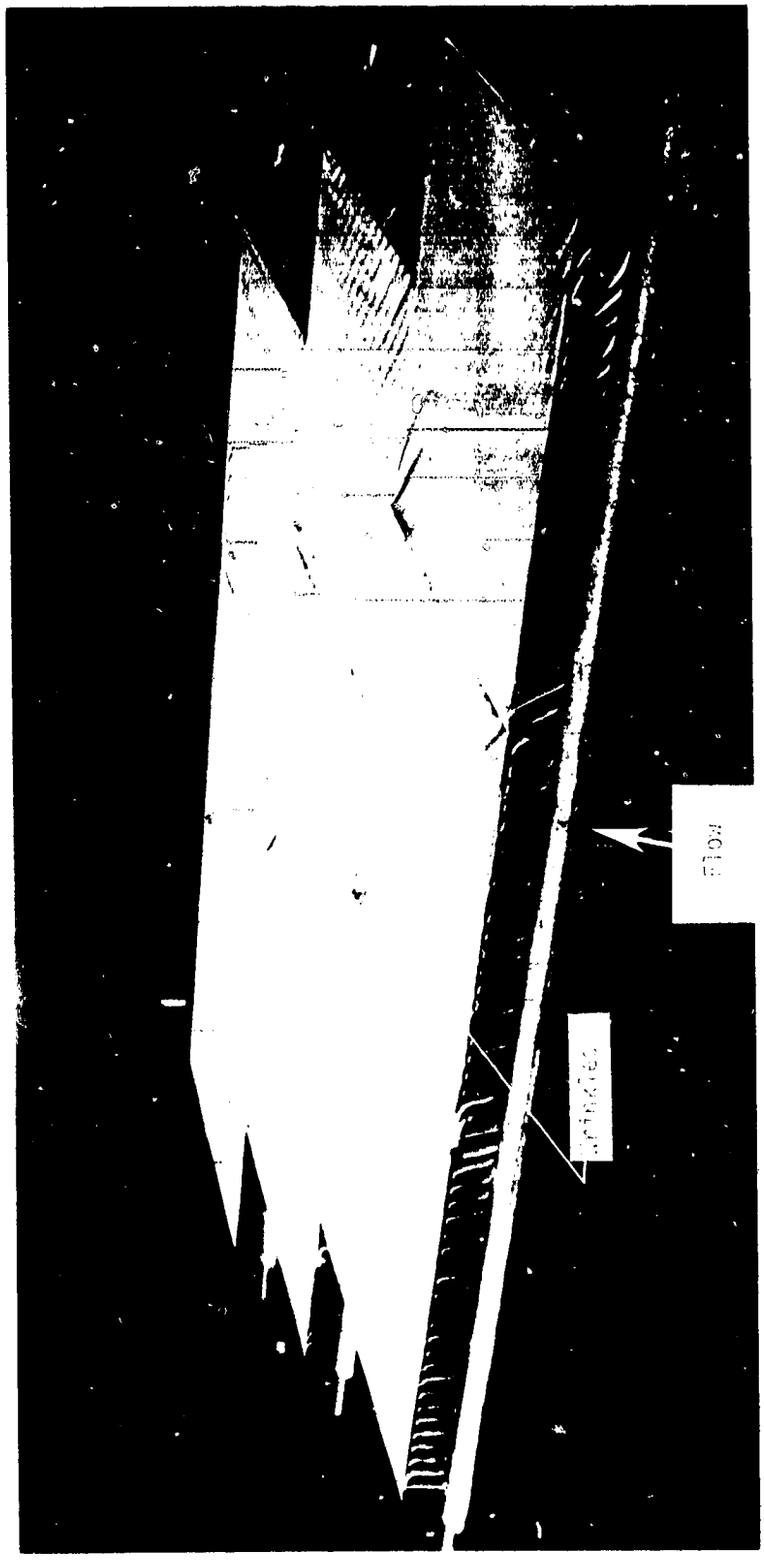


I-81-243

Figure 9.- Multiwall nine-tile model.

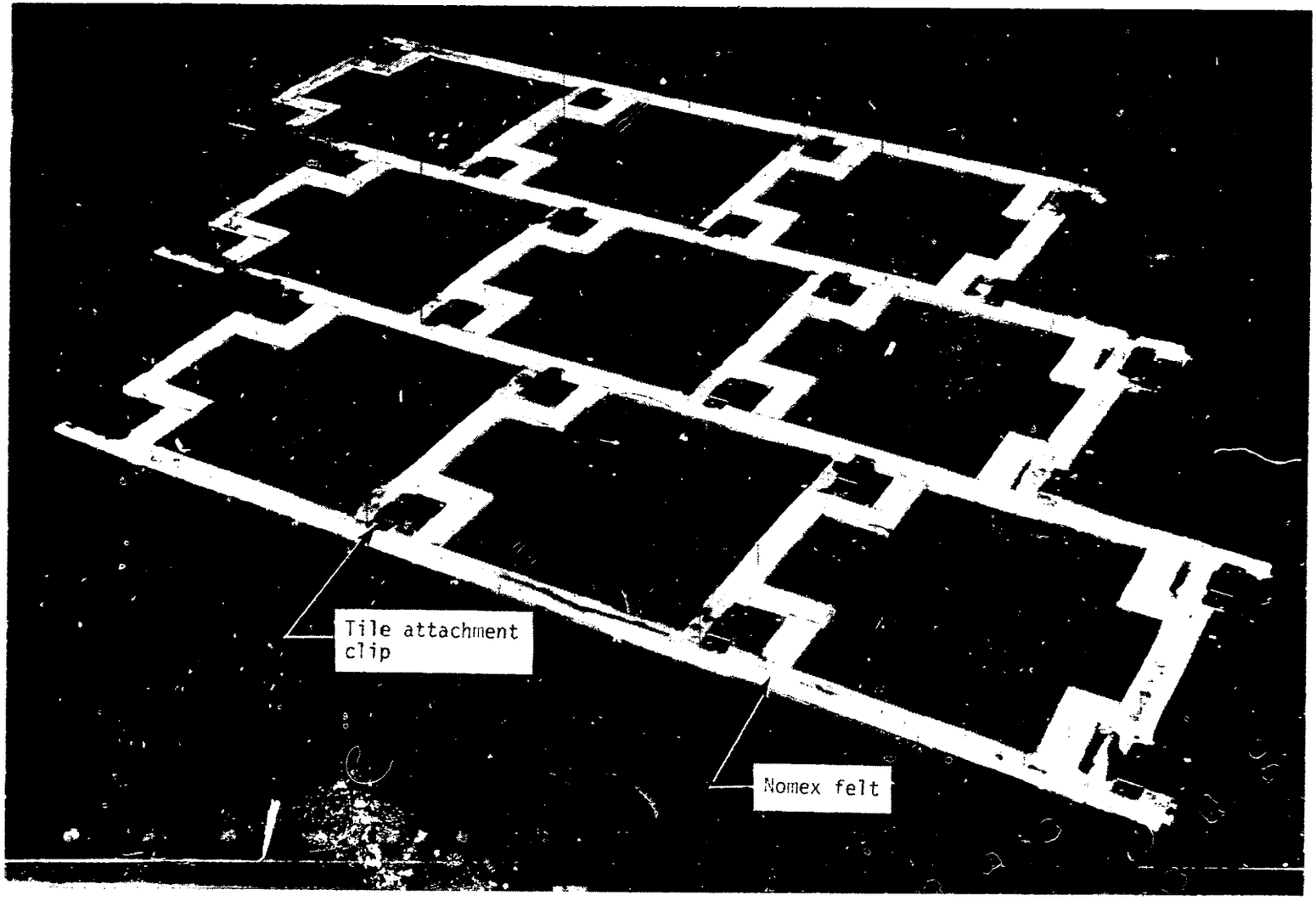


L-81-244

Figure 10.- Nomex flow inhibitor grid and tile attachment brackets for nine-tile model.

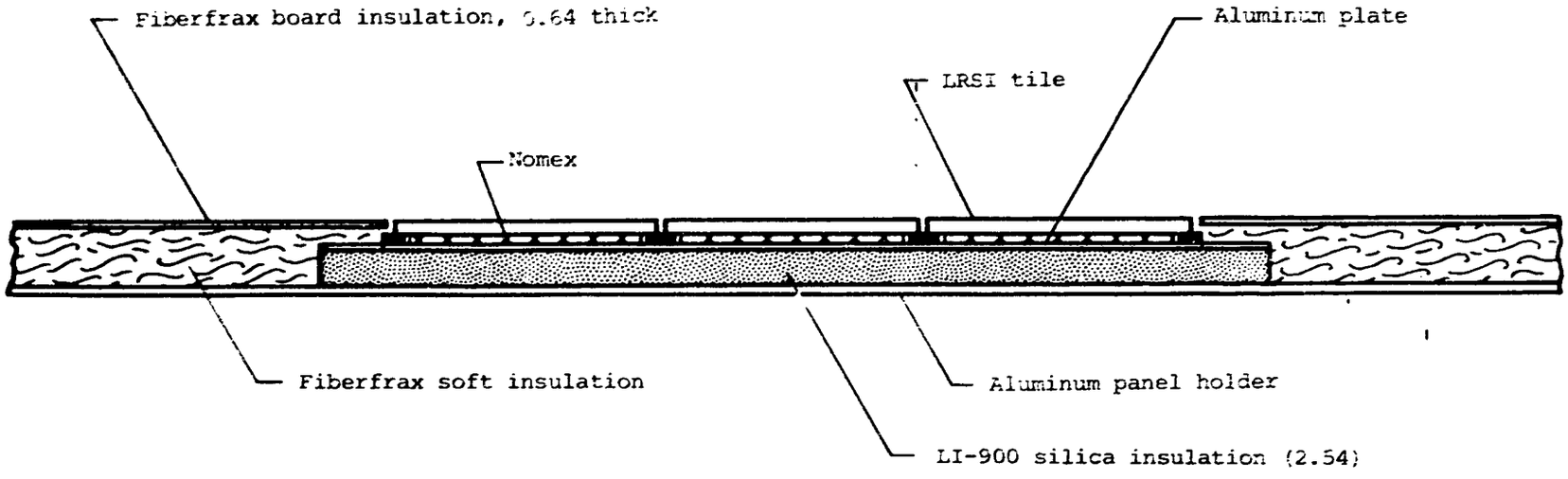


**Figure 11.- LRSI model test configuration. Dimensions are in centimeters.**

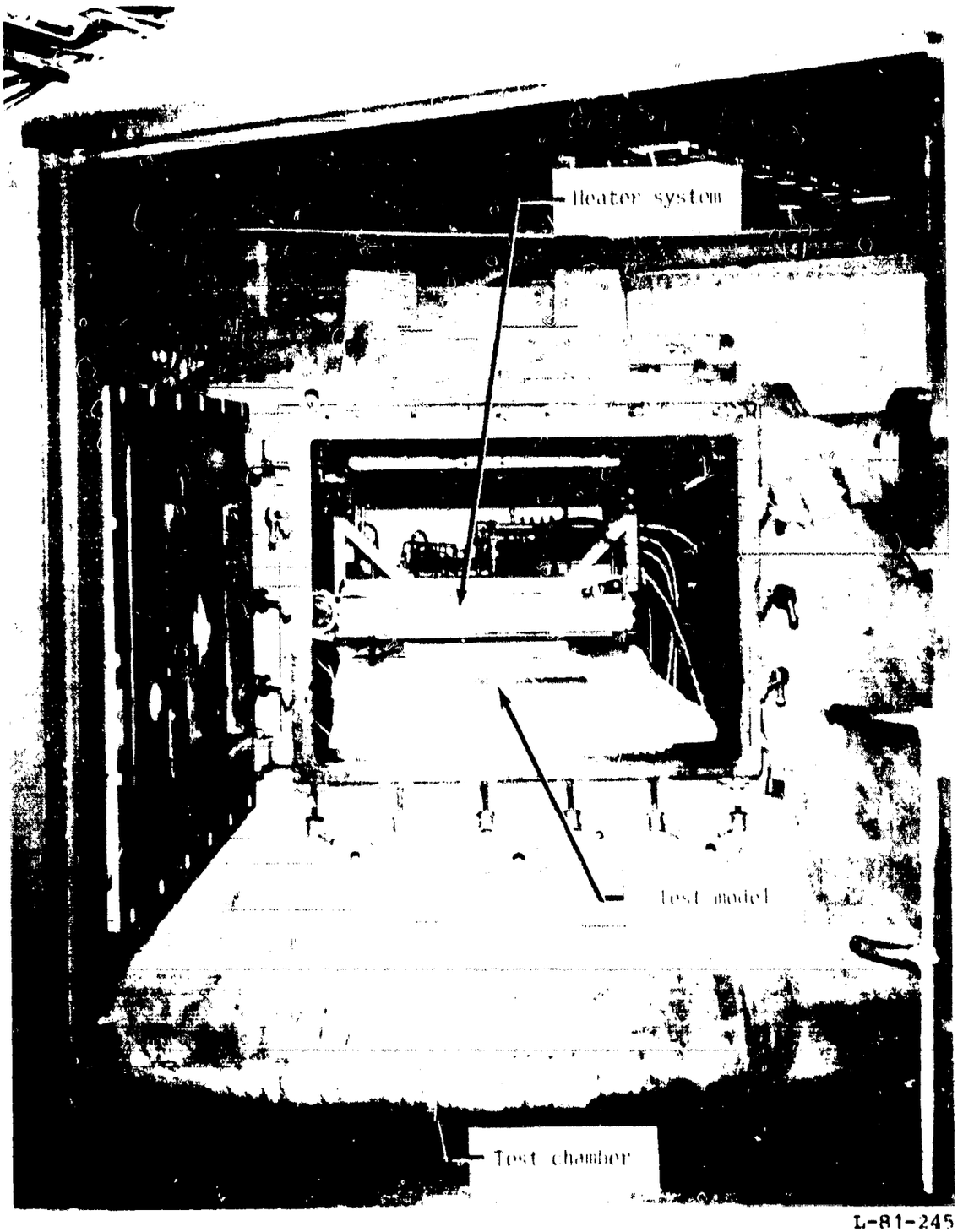


Figure 12.- Johnson Space Center Building 13 radiant heating test chamber.

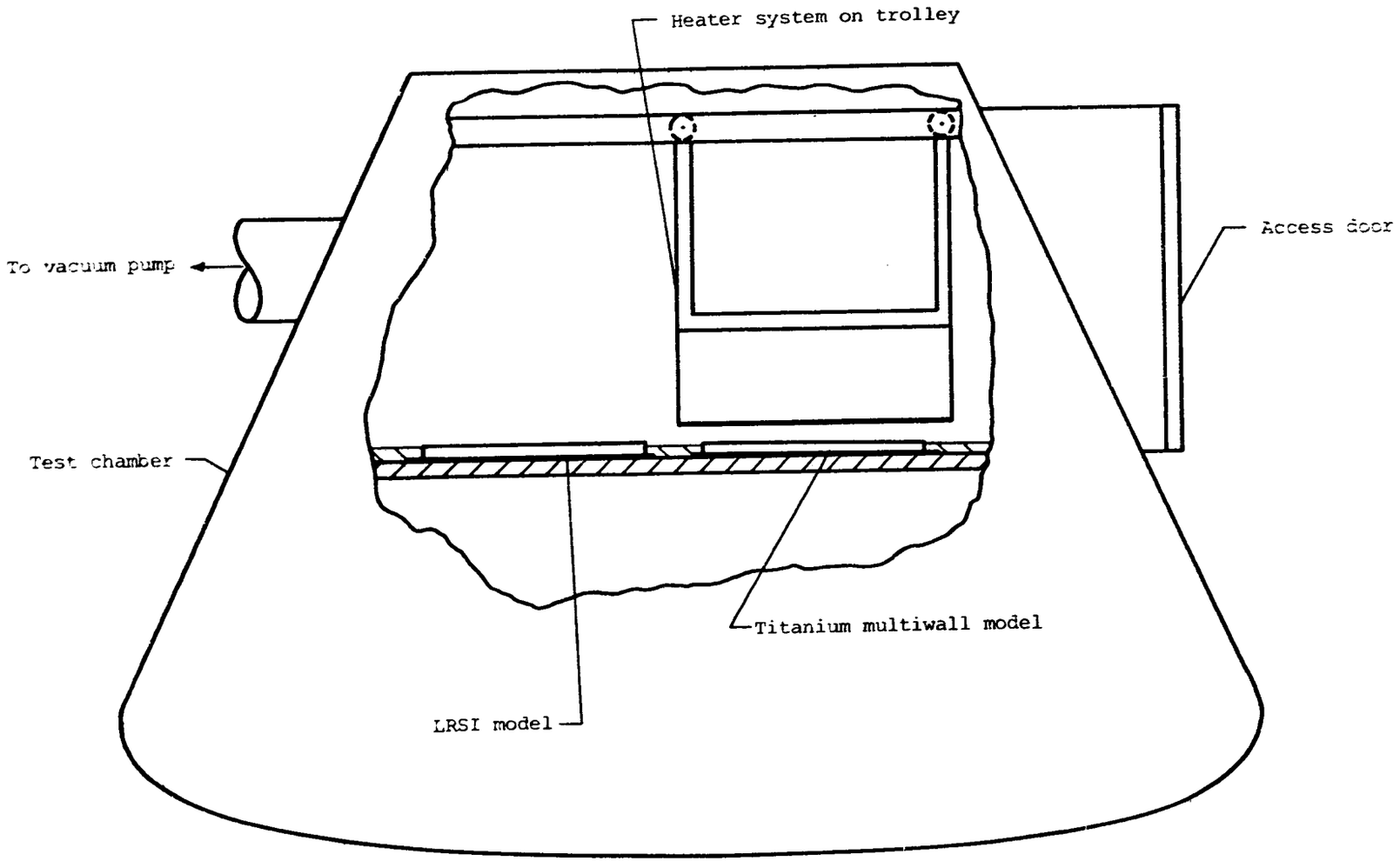


Figure 13.- Schematic drawing of JSC Building 13 radiant heating test chamber.

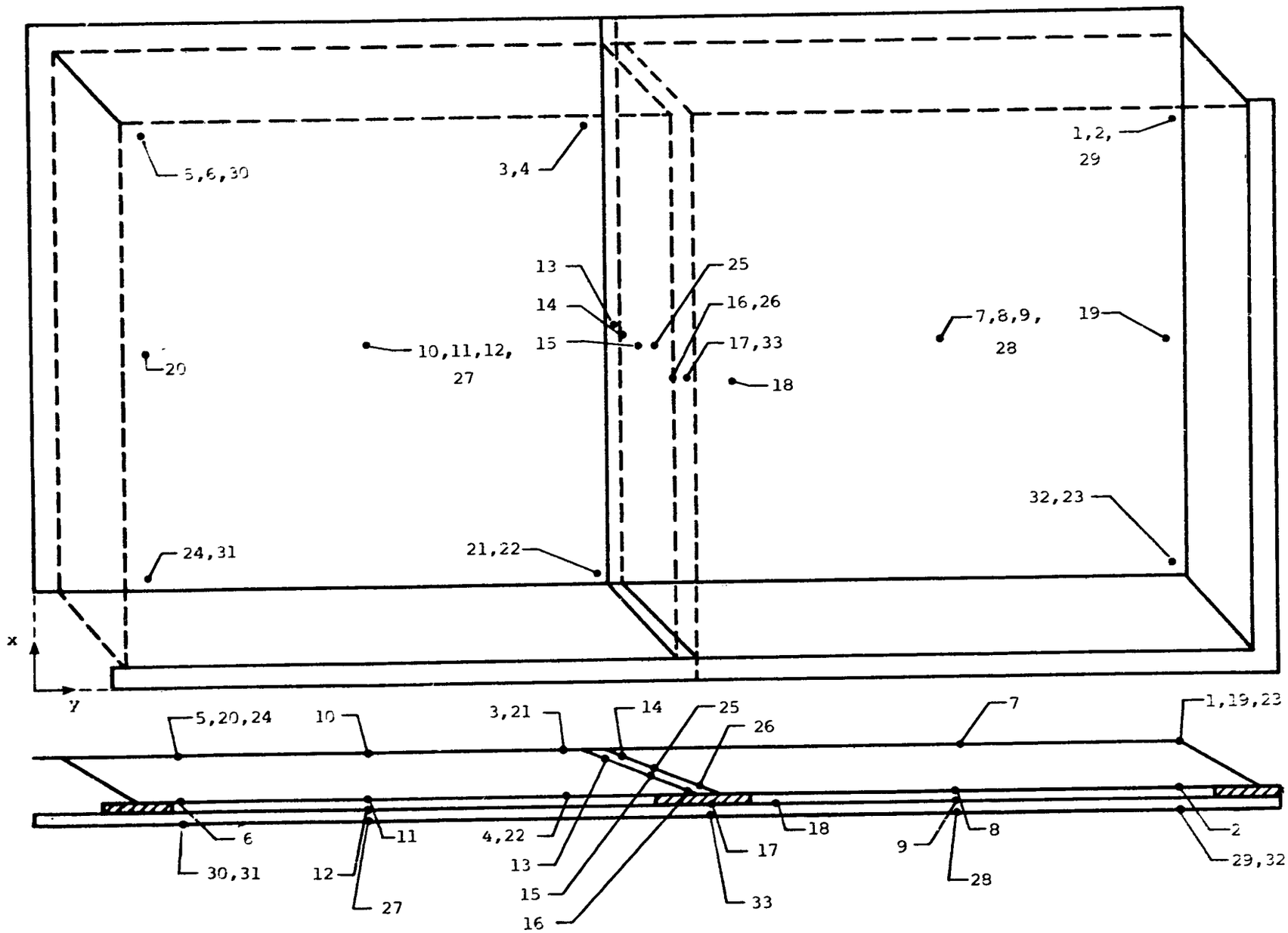


Figure 14.- Thermocouple locations on multiwall two-tile model.

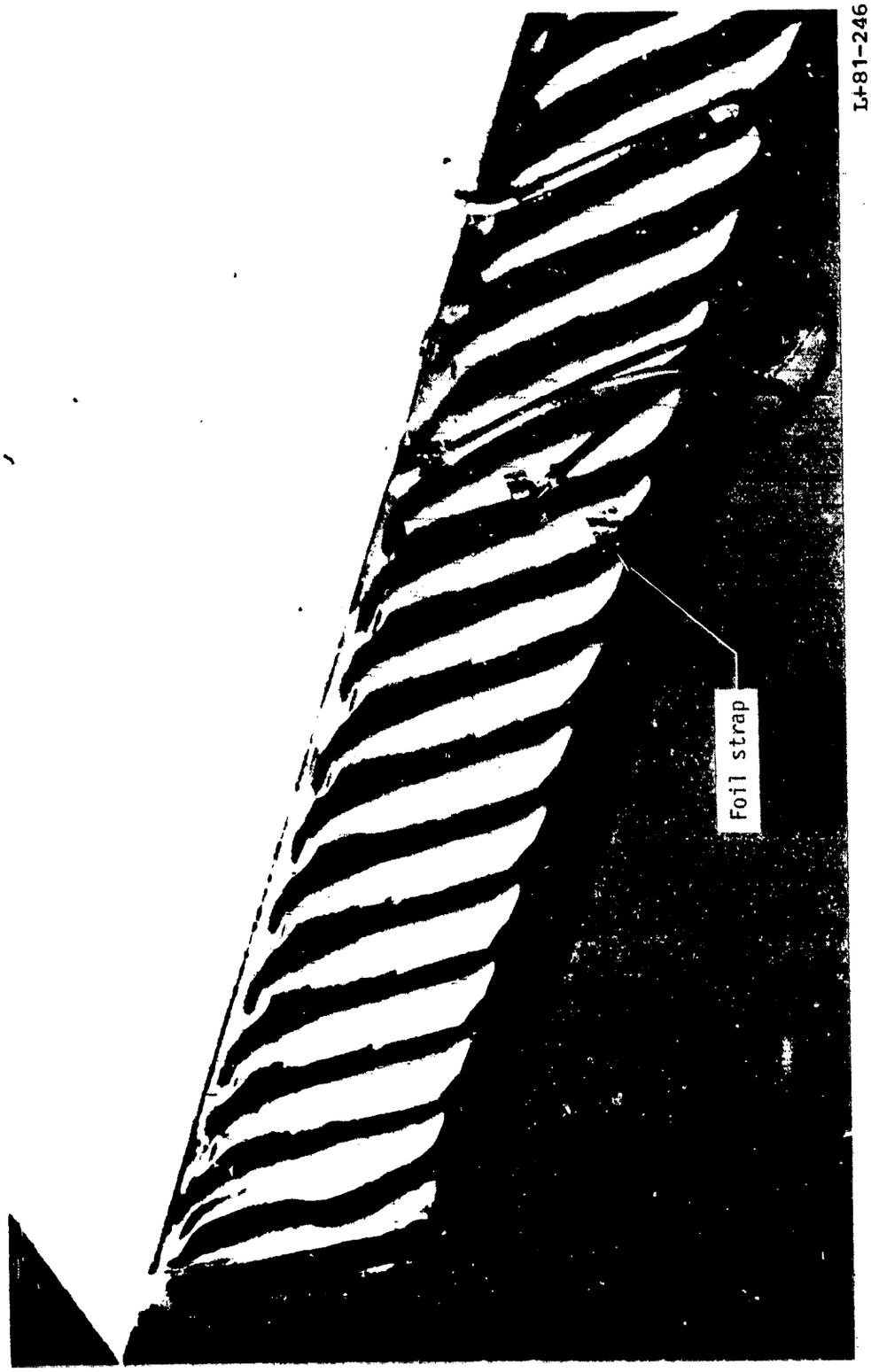


L-81-246

Figure 15.- Typical thermocouple installation.

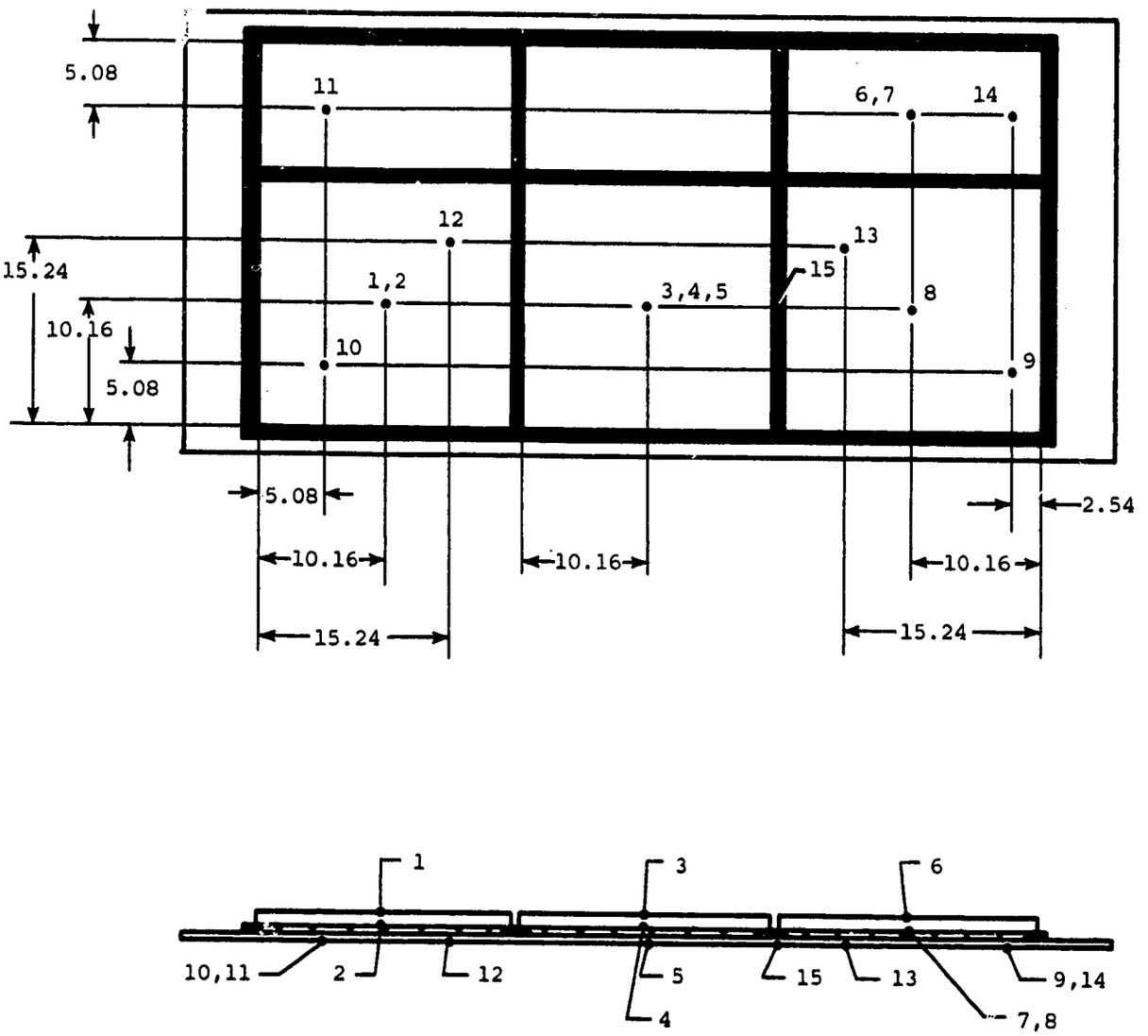


Figure 16.- LRSI model thermocouple locations.
Dimensions are in centimeters


Figure 17.- Multiwall nine-tile model installed in panel holder of 8' HTST.

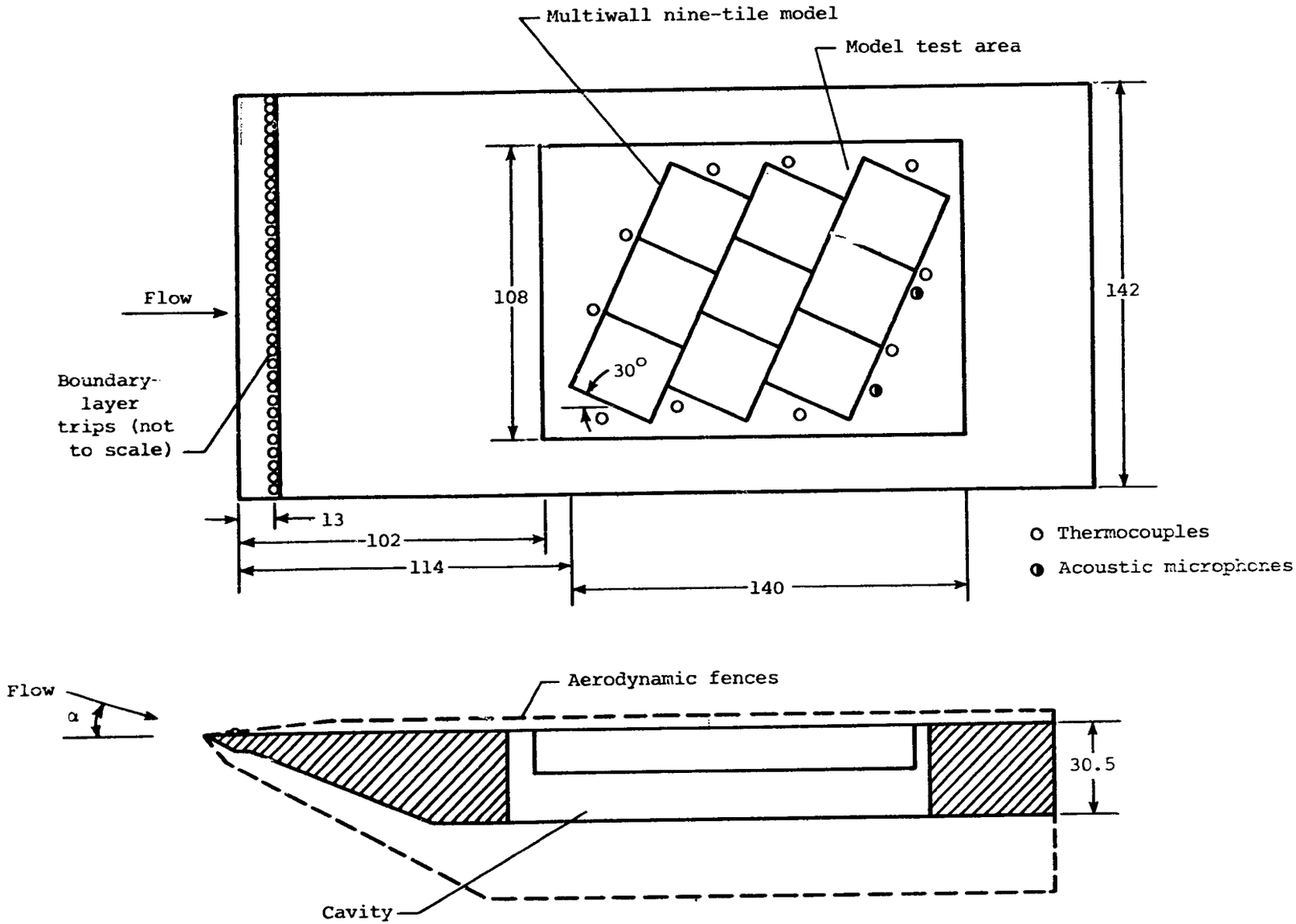


Figure 18.- Panel holder with instrumentation and nine-tile model installed. Dimensions are in centimeters.

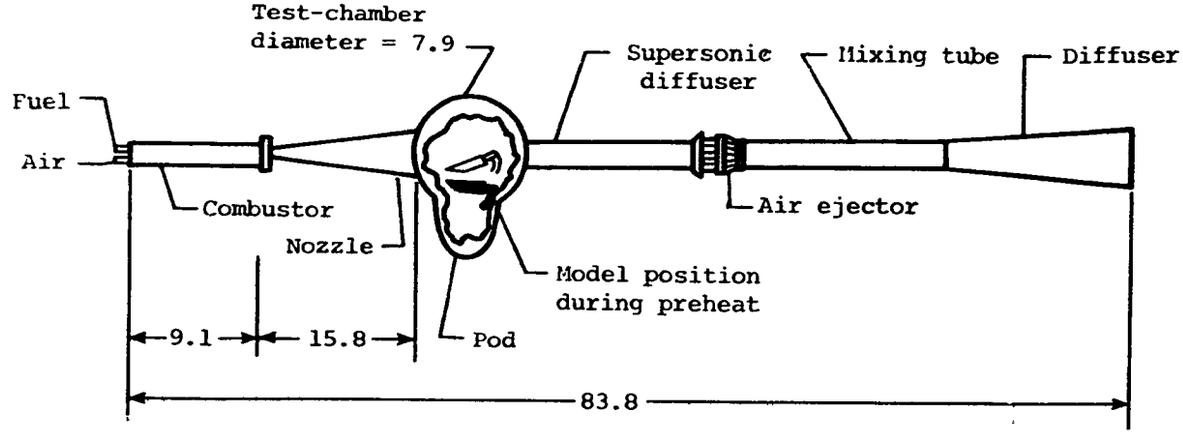


(a) Schematic of tunnel.

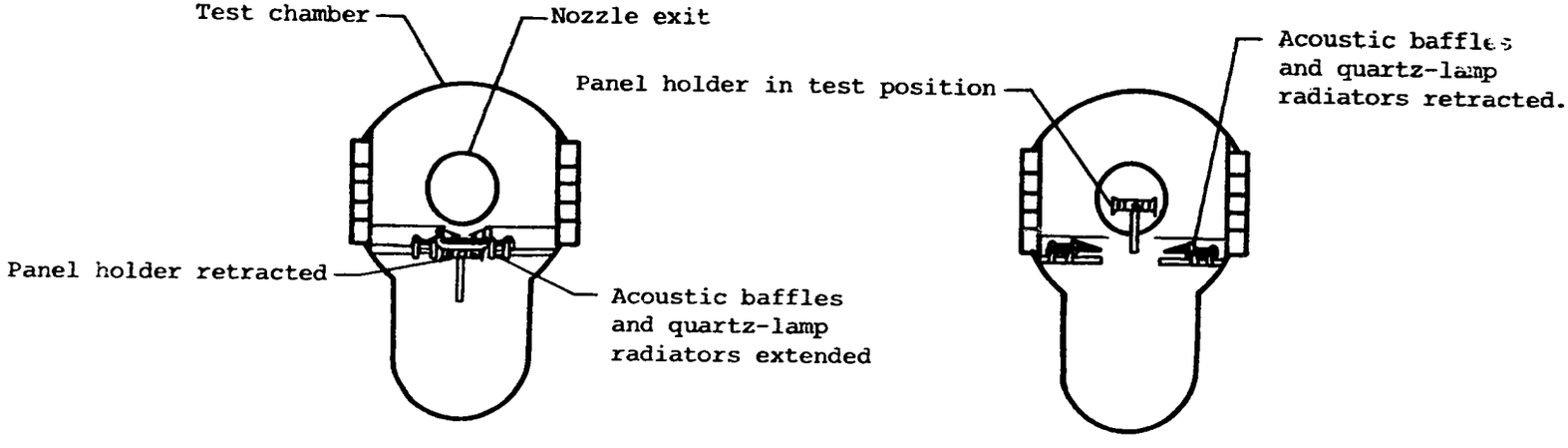


(b) Model position during preheat.

(c) Model position during test.

Figure 19.- Schematic of Langley 8-Foot High-Temperature Structures Tunnel.
Dimensions are in meters.

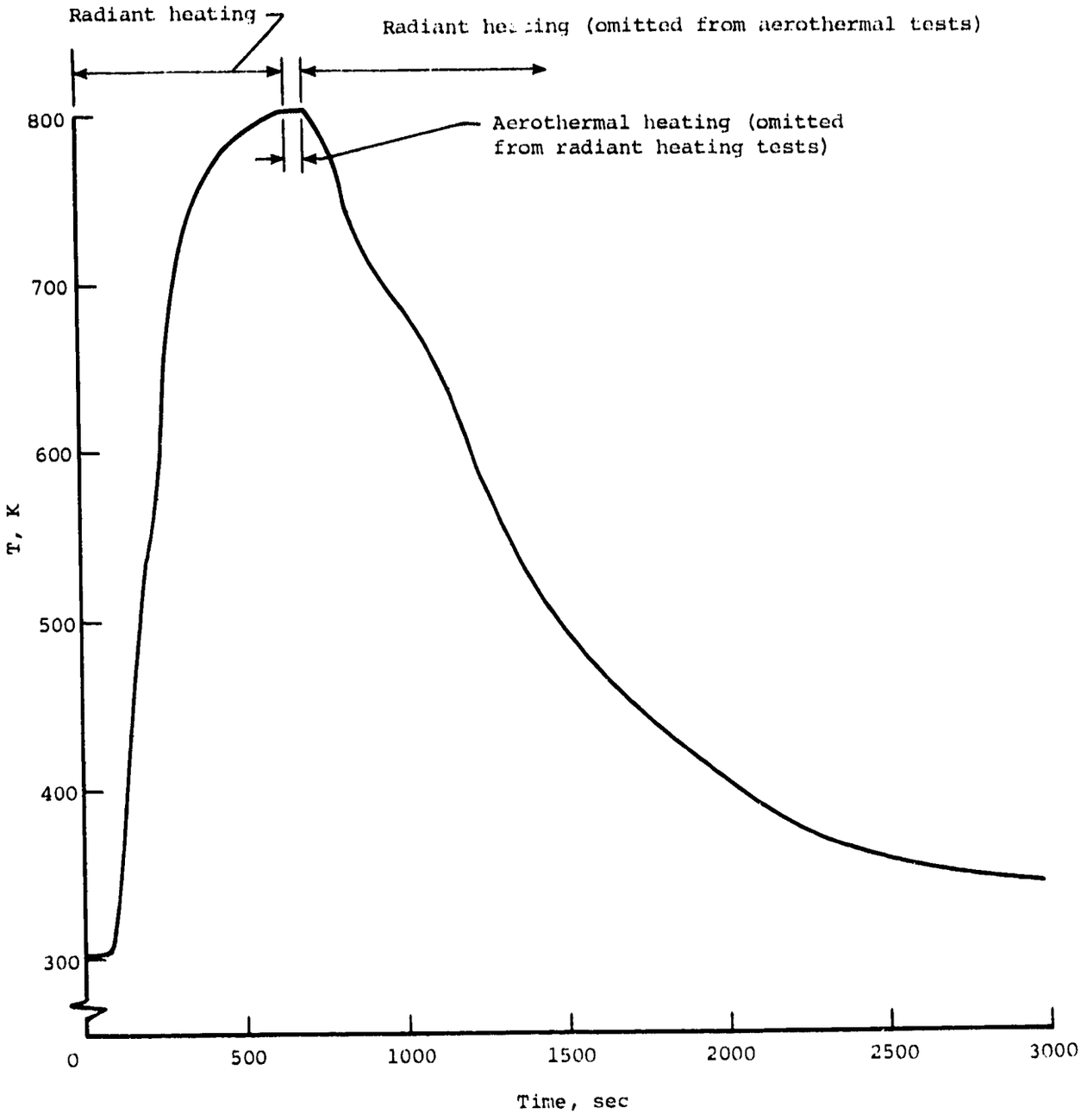


Figure 20.- Typical temperature history for nine-tile model.

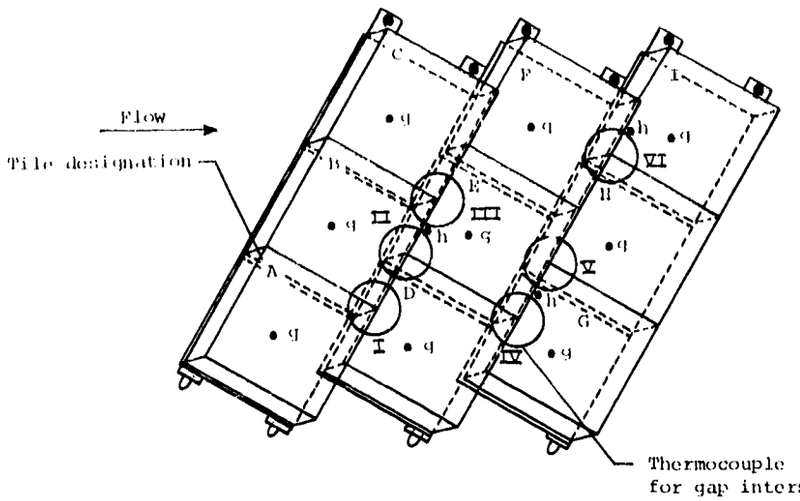


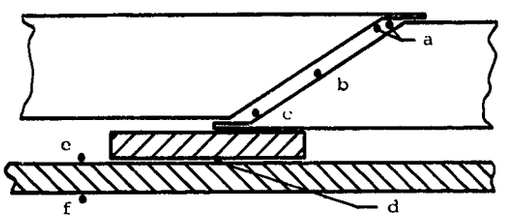


Gap intersection

- • Thermocouple
- a 0.64 cm below top surface
- b Midpoint of slope
- c 0.64 cm above bottom surface
- d Primary structure under Nomex felt
- e Primary structure
- f Backside of primary structure
- g Backside of multiwall panel
- h Top surface of multiwall panel

| Thermocouple | Tile | Thermocouple location (a) | Thermocouple | Tile | Thermocouple location (a) |
|---|---|---|---|---|---|
| 1 | D | I,a | 27 | E | V,e |
| 2 | B | I,a | 28 | I | VI,a |
| 3 | A | I,a | 29 | F | VI,a |
| 4 | D | I,b | 30 | I | VI,b |
| 5 | D | I,c | 31 | I | VI,c |
| 6 | A | I,d | 32 | F | VI,d |
| 7 | A | I,e | 33 | F | VI,e |
| 8 | E | III,a | 34 | A | g |
| 9 | C | III,a | 35 | B | g |
| 10 | B | III,a | 36 | C | g |
| 11 | E | III,b | 37 | D | g |
| 12 | E | III,c | 38 | E | g |
| 13 | B | III,d | 39 | F | g |
| 14 | B | III,e | 40 | G | g |
| 15 | G | IV,a | 41 | H | g |
| 16 | D | IV,a | 42 | I | g |
| 17 | G | IV,b | 43 | E | h |
| 18 | G | IV,c | 44 | G | h |
| 19 | D | IV,d | 45 | I | h |
| 20 | D | IV,e | 46 | E | II,a |
| 21 | H | V,a | 47 | E | II,b |
| 22 | G | V,a | 48 | E | II,c |
| 23 | E | V,a | 49 | D | II,a |
| 24 | H | V,b | 50 | A | f |
| 25 | H | V,c | 51 | E | f |
| 26 | E | V,d | 52 | F | f |

[a] x, y: x = Gap intersection, y = Thermocouple position.

Figure 21.- Thermocouple distribution for nine-tile model.

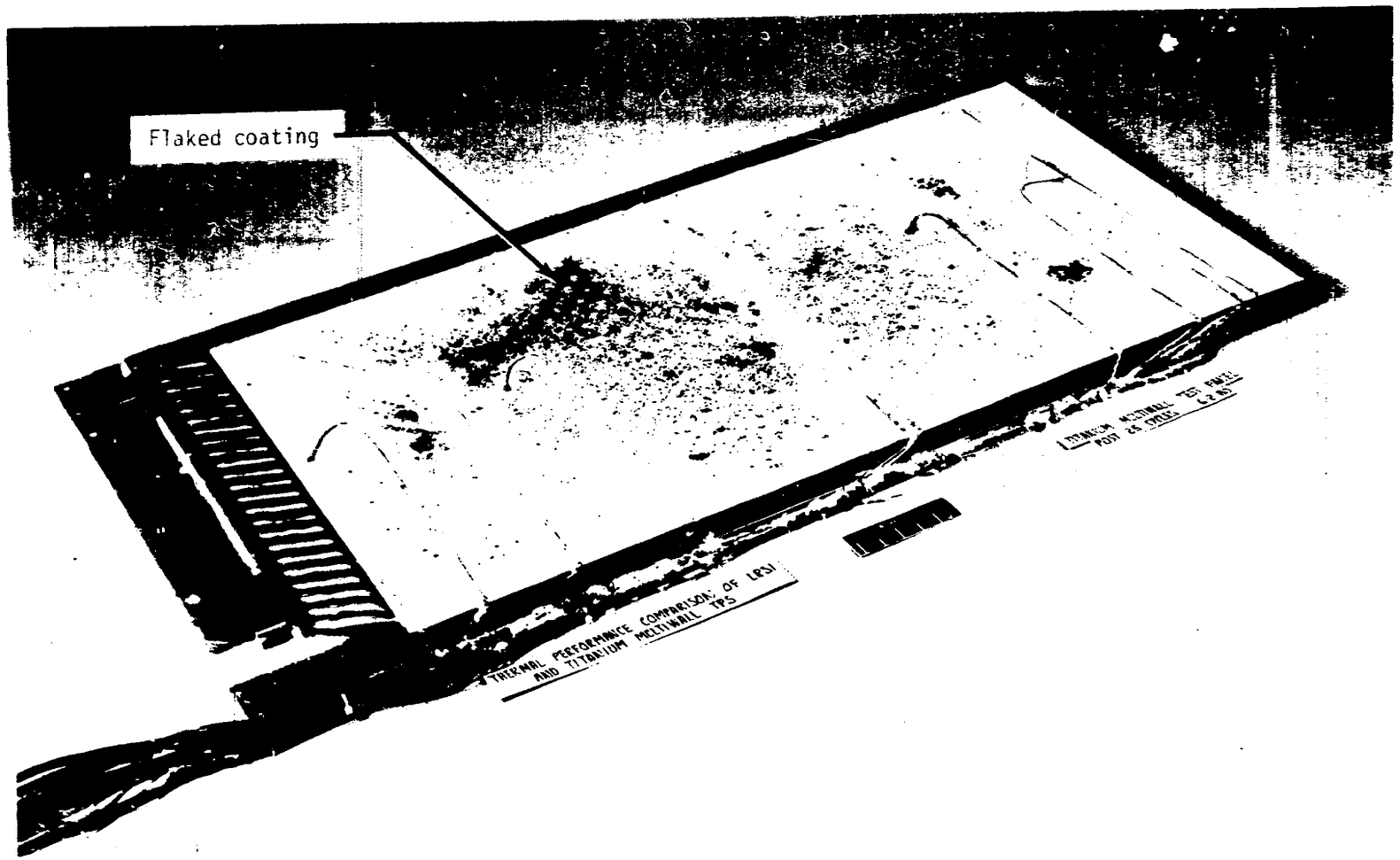


L-81-248

Figure 22.- Multiwall two-tile model after 25 thermal tests.

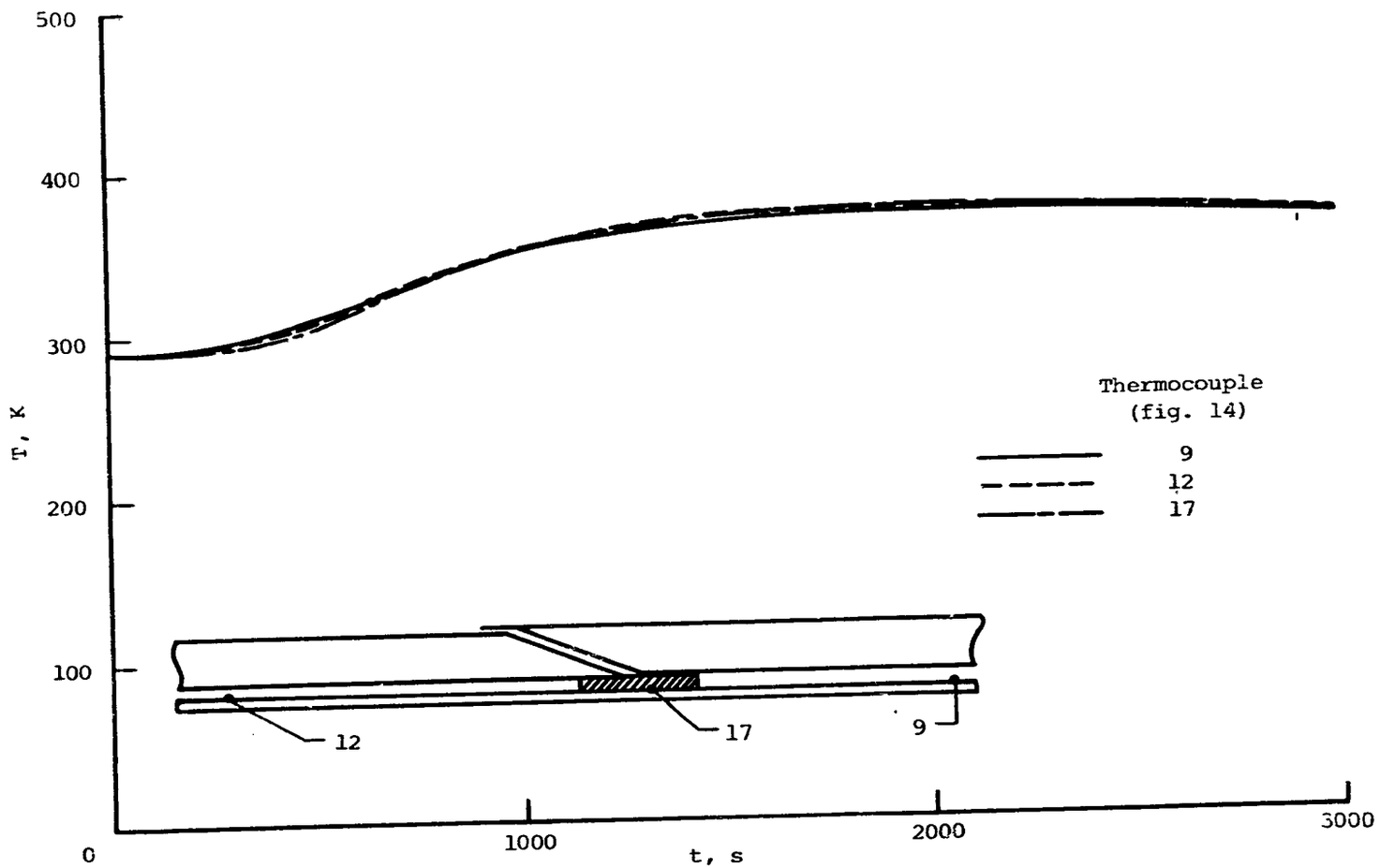


Figure 23.- Temperature of primary structure under multiwall tiles and under scarf joint of two-tile model (test 1).

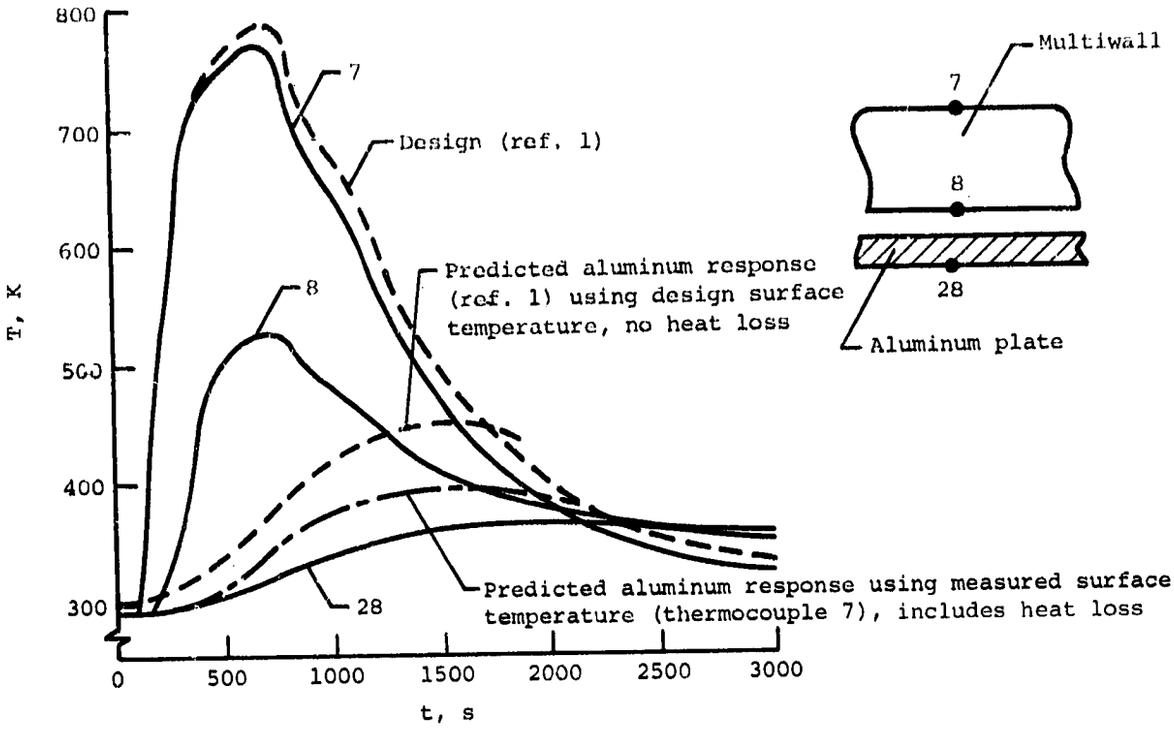


(a) Multiwall TPS.

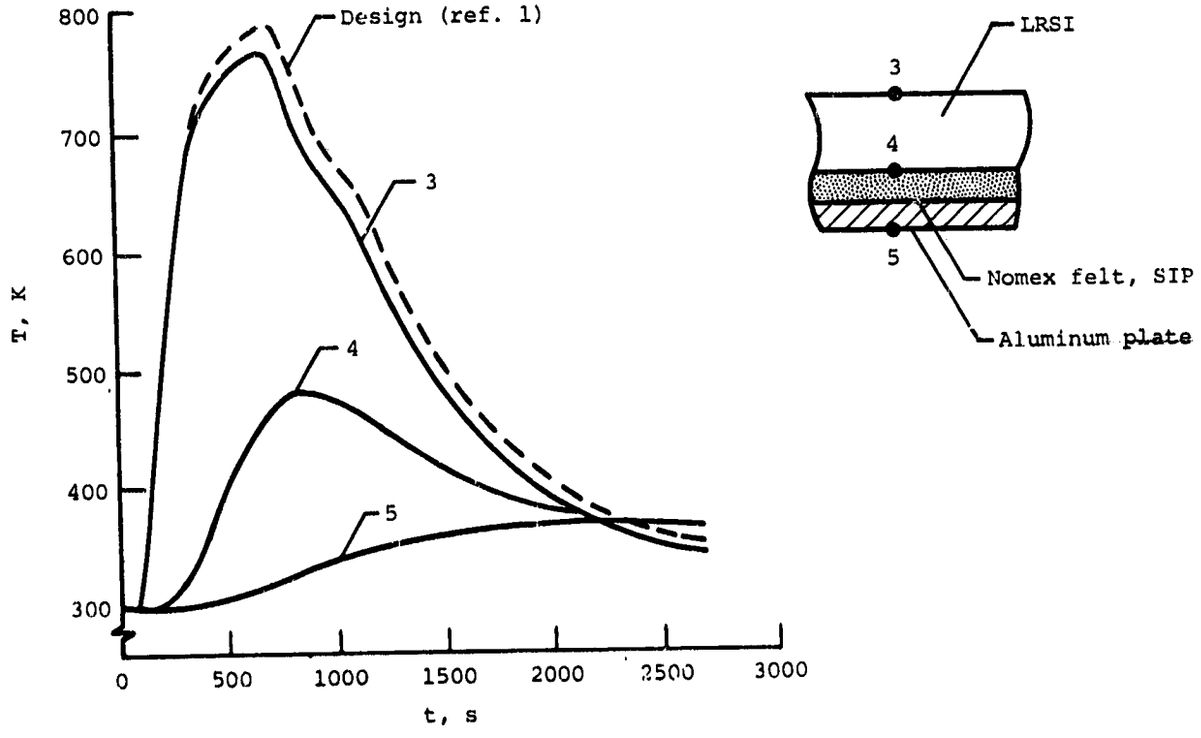


(b) LRSI.

Figure 24.- Temperature histories for cyclic radiant heating through models (test 1).

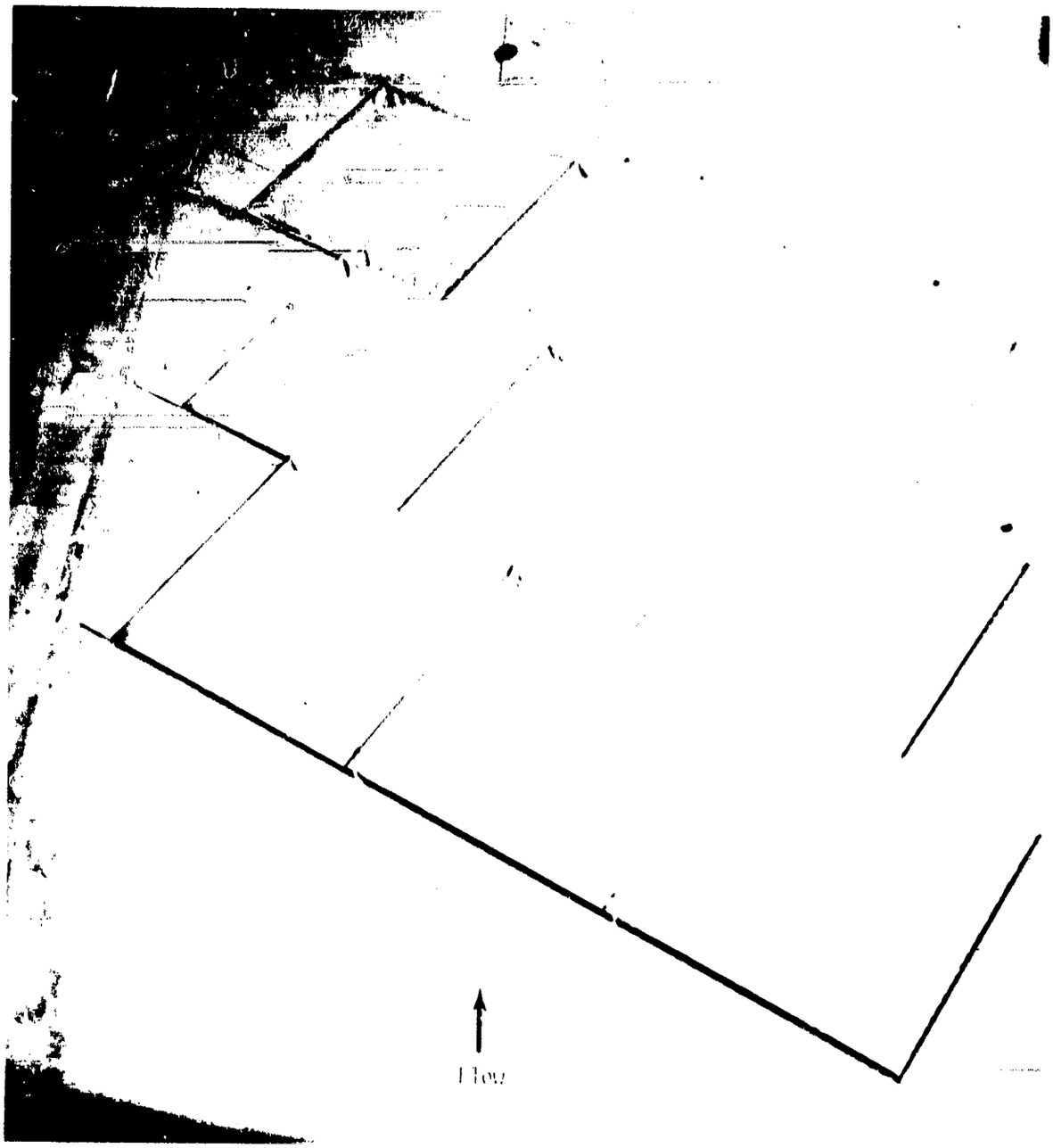


L-81-249

Figure 25.- Nine-tile model after three coating cure cycles.

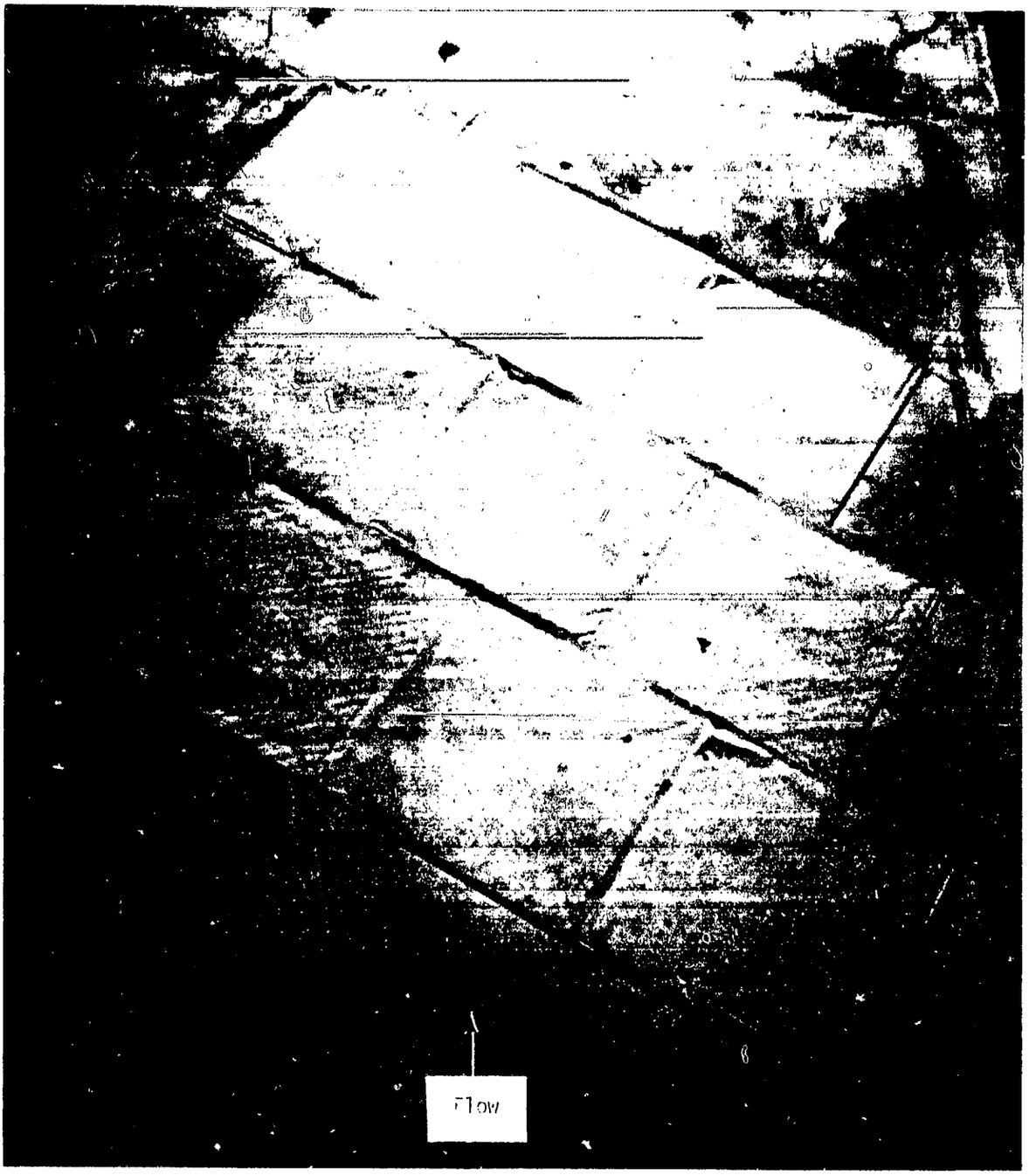


L-81-250

Figure 26.- Nine-tile model at end of test series.

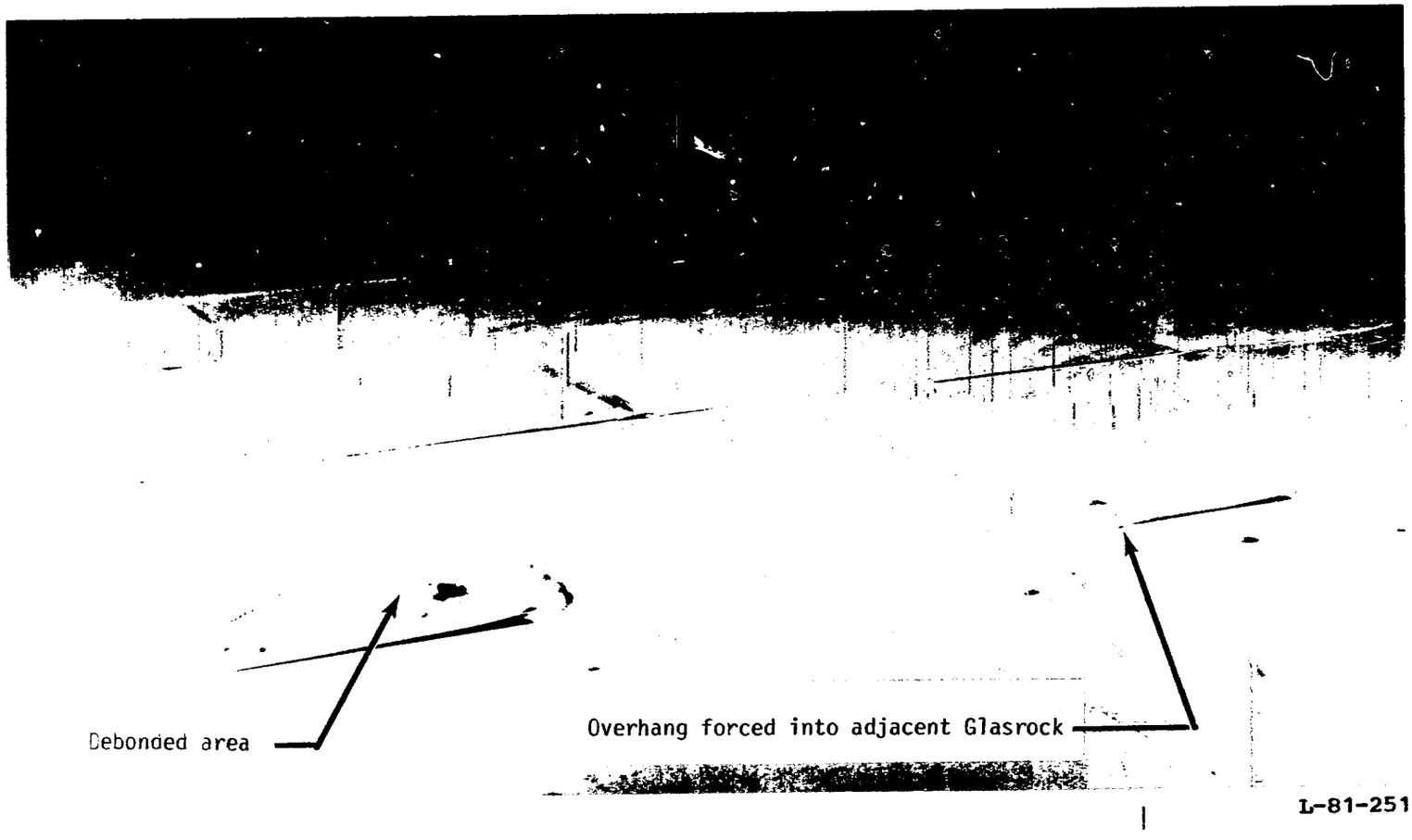


(a) Surface debonding.

Figure 27.- Debonding of multiwall face sheets.


L-81-252

(b) Backface debonding.

Figure 27.- Concluded.

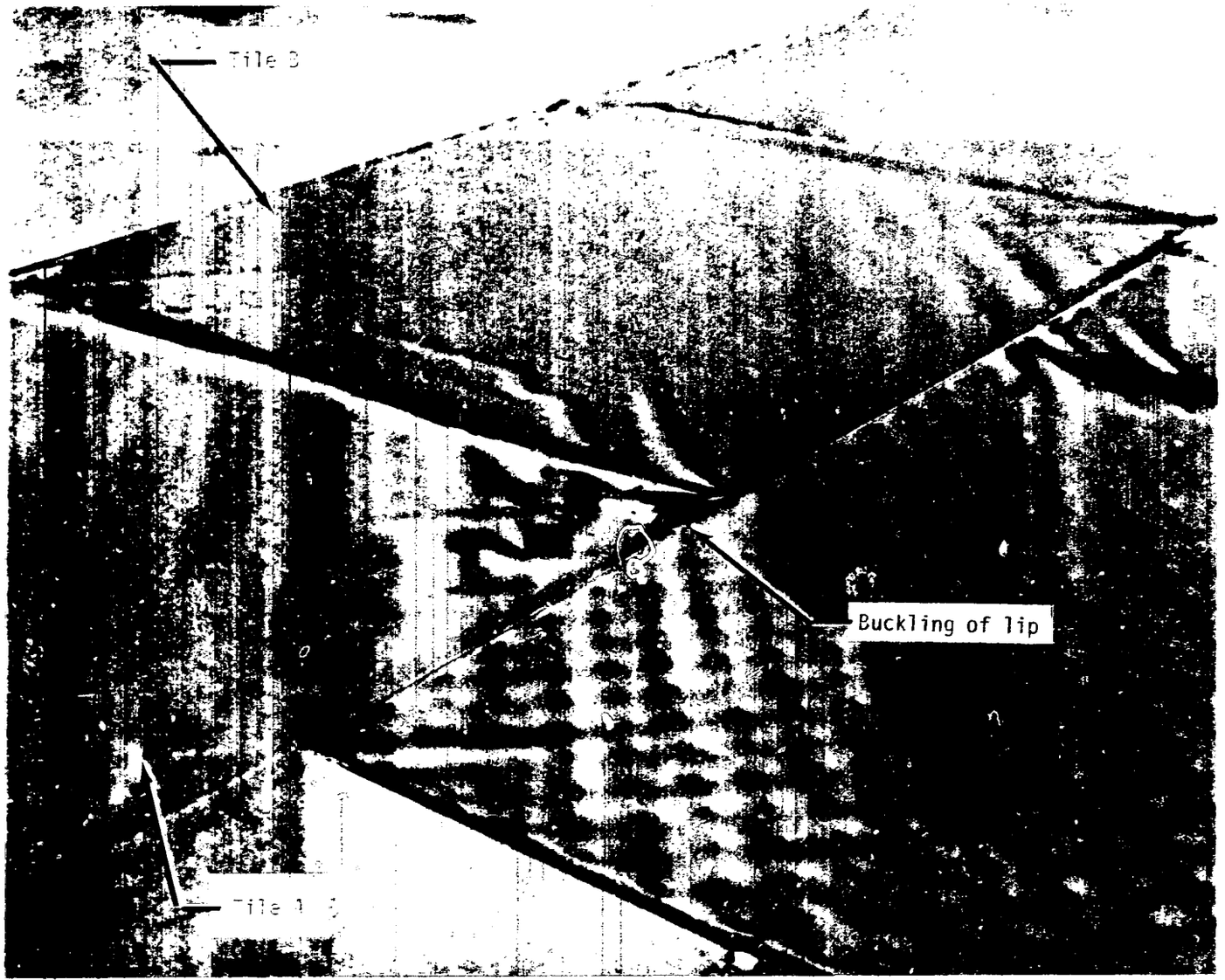


L-81-253

**Figure 28.- Buckling of tile trailing-edge lip.**

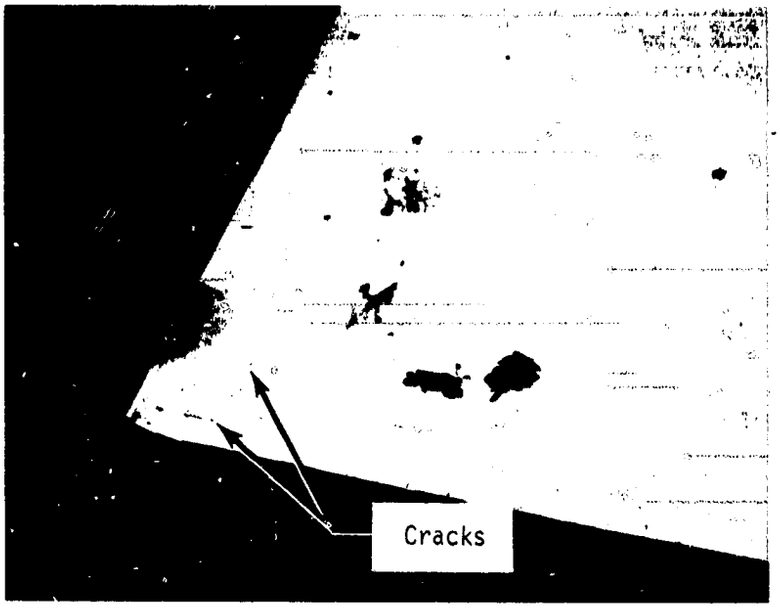


(a) Top surface cracks.

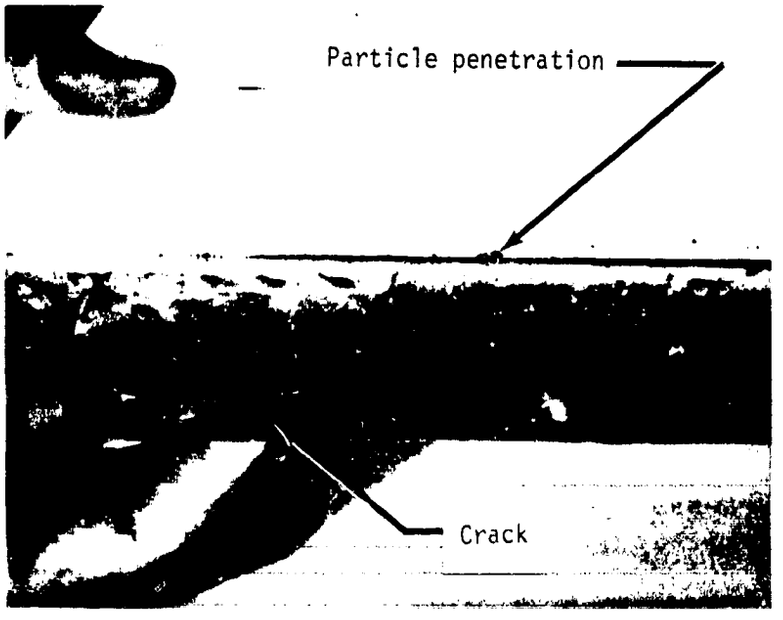


L-81-254

(b) Cracks along lower surface lip.

Figure 29.- Nine-tile model damage on tile 7.

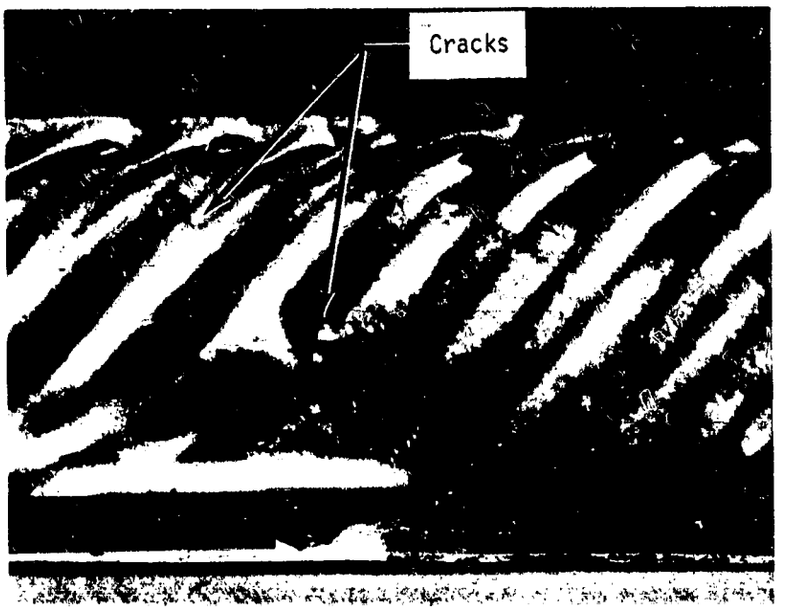


L-81-255

(c) Cracks in corrugated edge closure.

Figure 29.- Concluded.

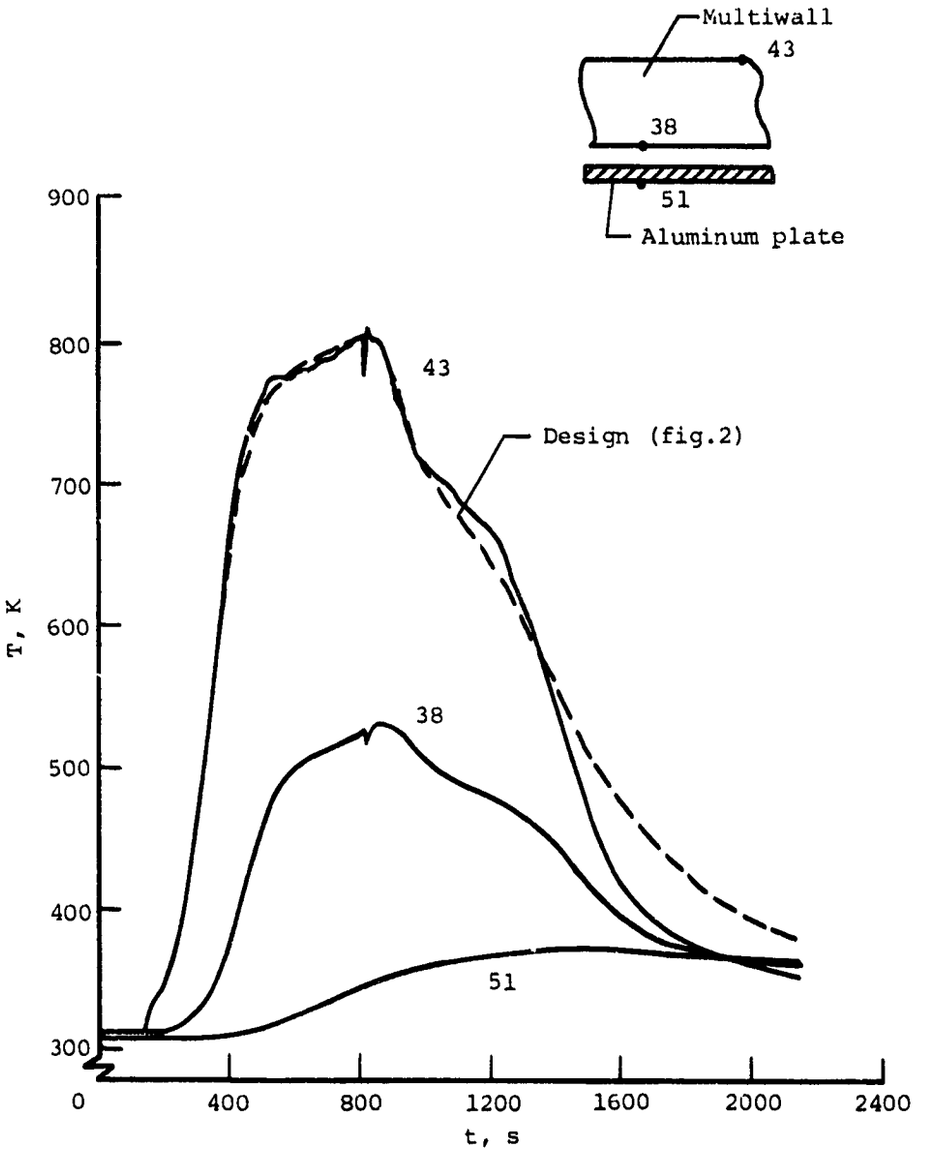


(a) Radiant heating (test 9).

Figure 30.- Temperature history at center of model.

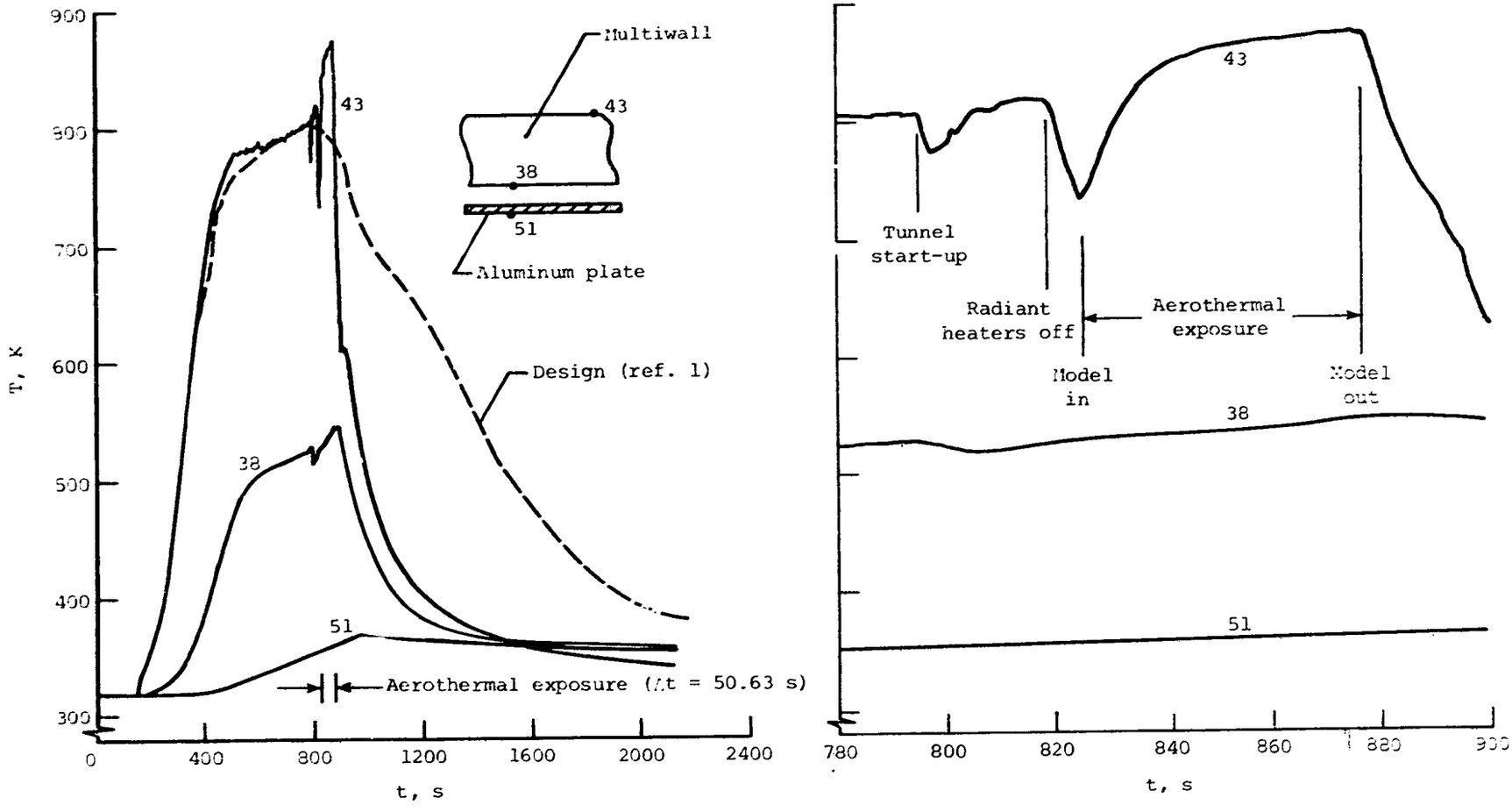


(b) Aerothermal heating (test 15).

Figure 30.- Concluded.

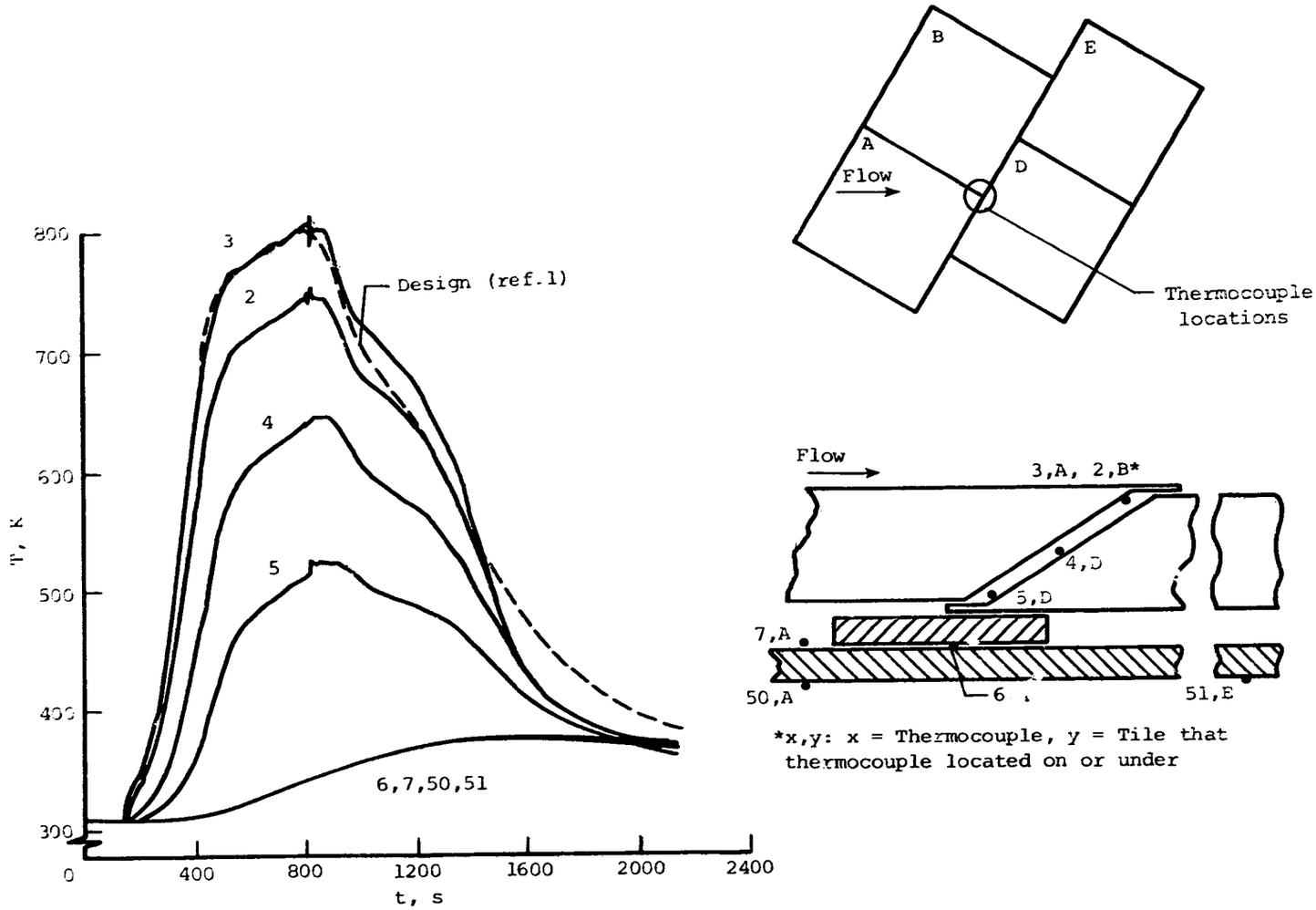


(a) Radiant heating at front of model (test 9).

Figure 31.- Gap heating where longitudinal gap terminates at transverse gap.

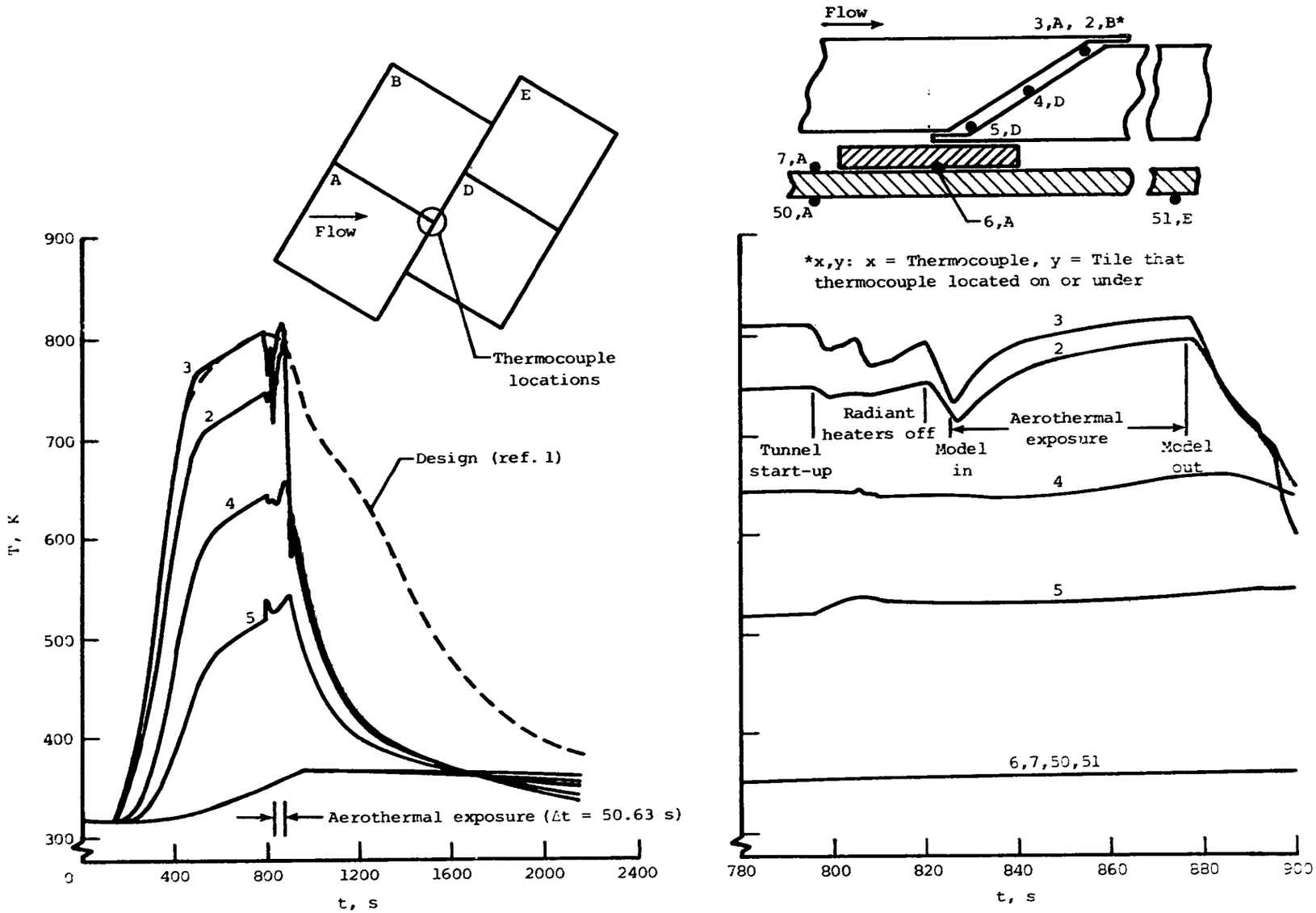


(b) Aerothermal heating at front of model (test 15).

Figure 31.- Continued.

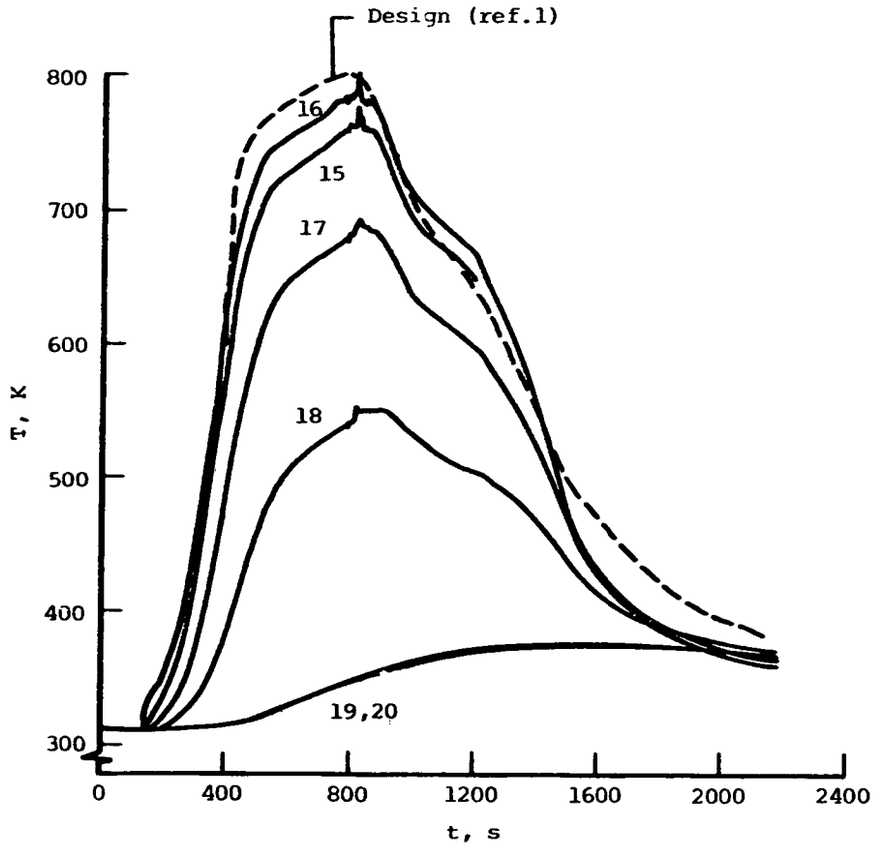


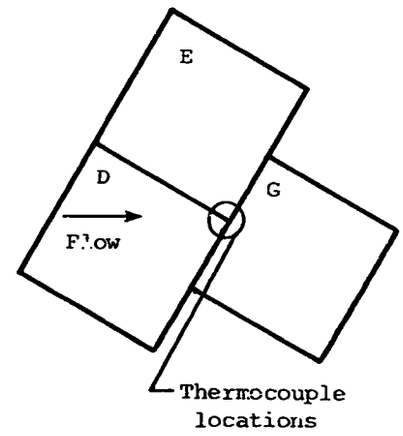


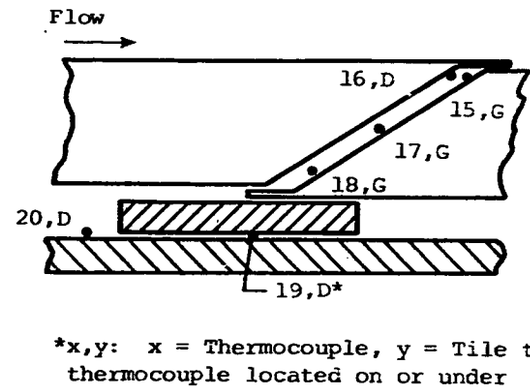


*x,y: x = Thermocouple, y = Tile that thermocouple located on or under

(c) Radiant heating at rear of model (test 9).

Figure 31.- Continued.

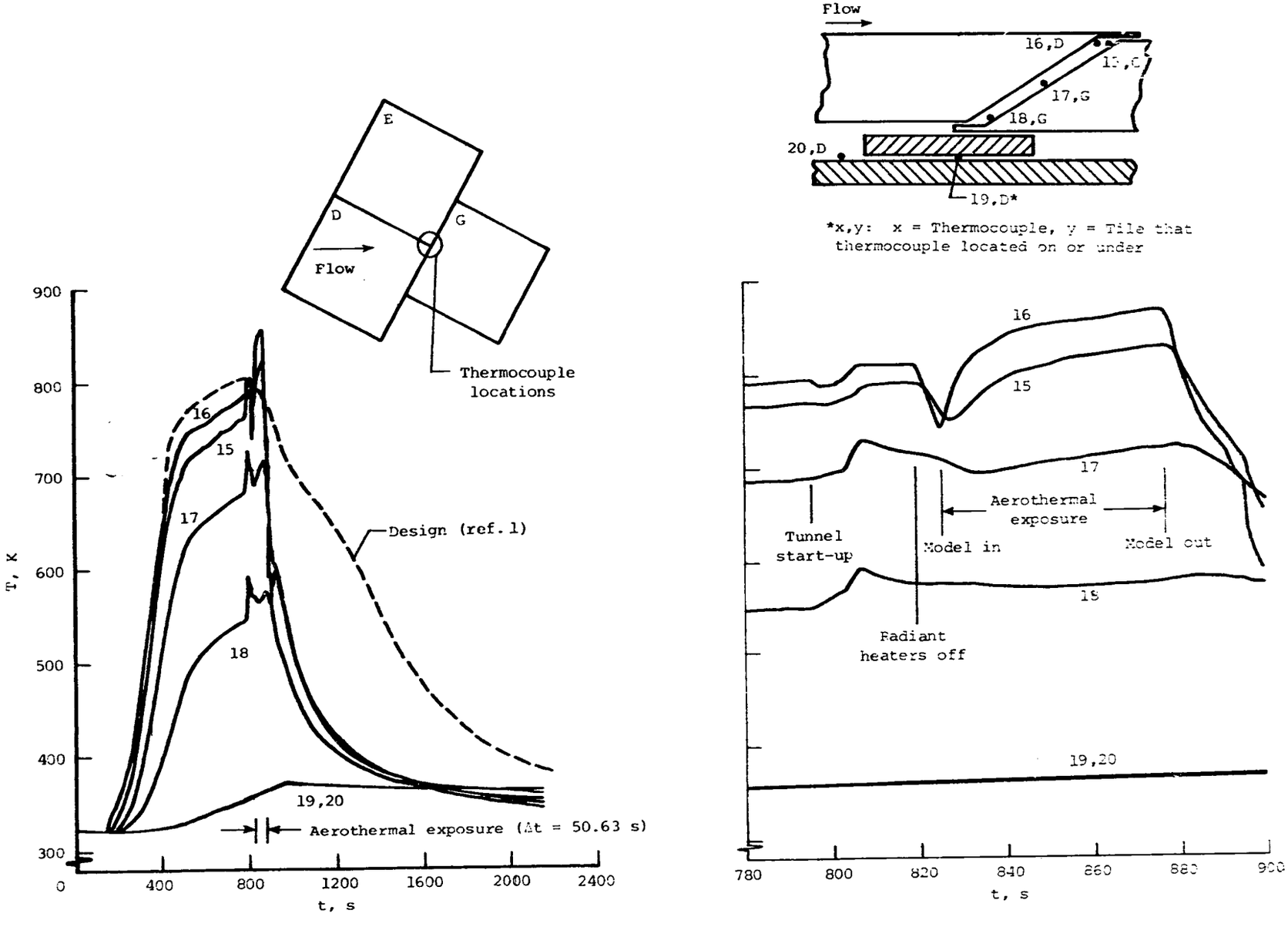


(d) Aerothermal heating at rear of model (test 15.)

Figure 31.- Concluded.

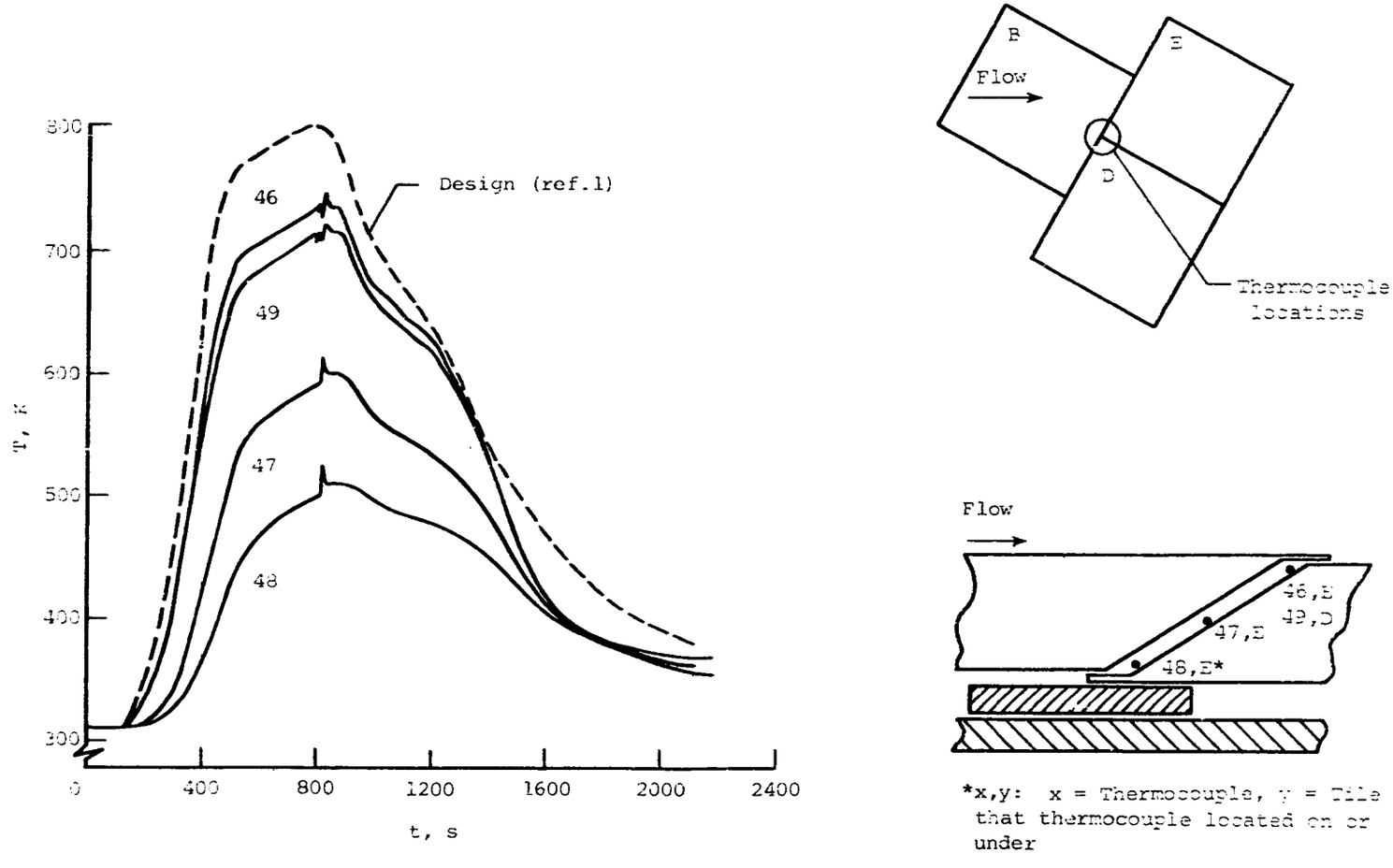


(a) Radiant heating (test 9).

Figure 32.- Gap heating where longitudinal gap originates at transverse gap.

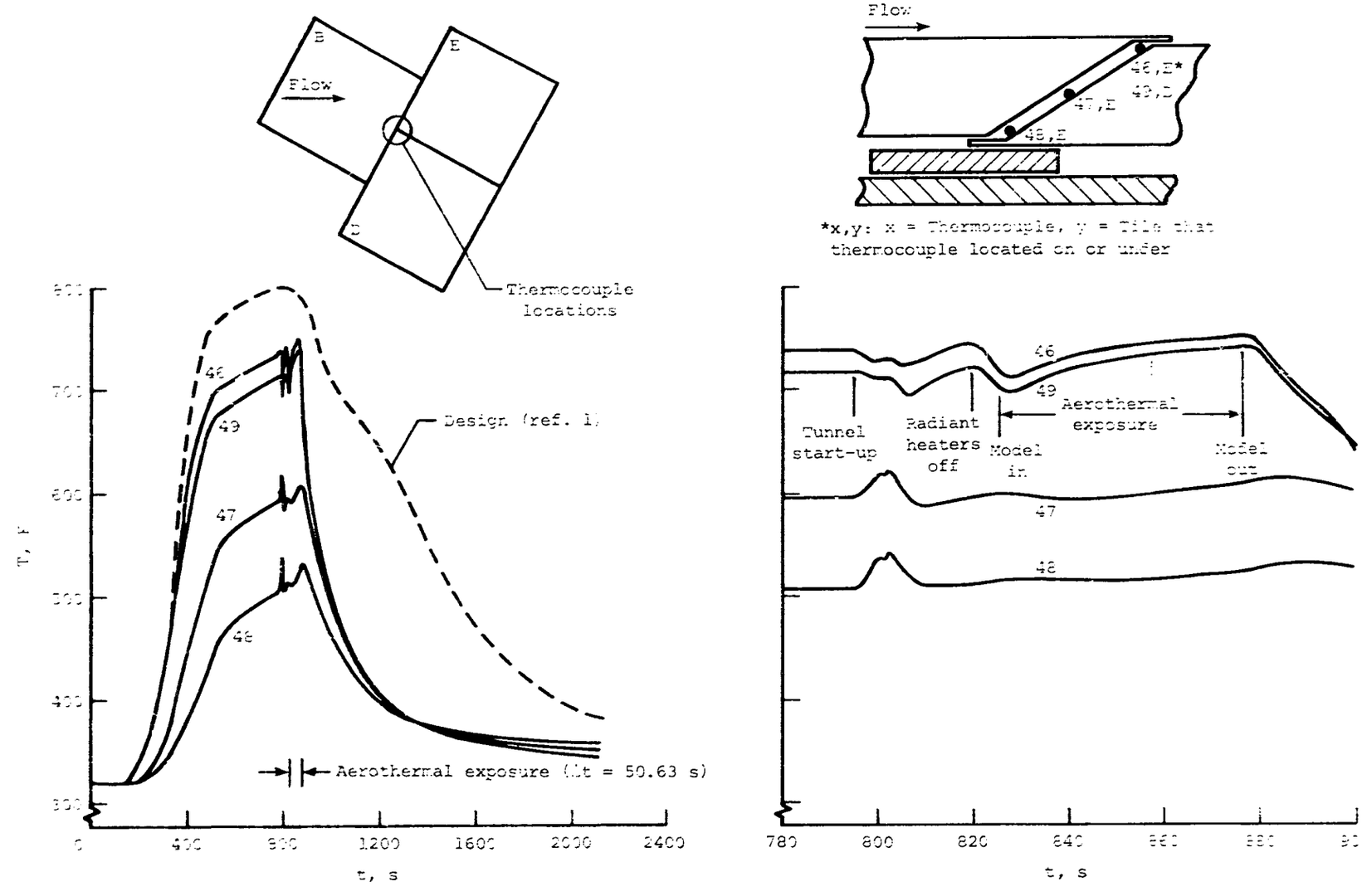


(b) Aerothermal heating (test 15).

Figure 32.- Concluded.

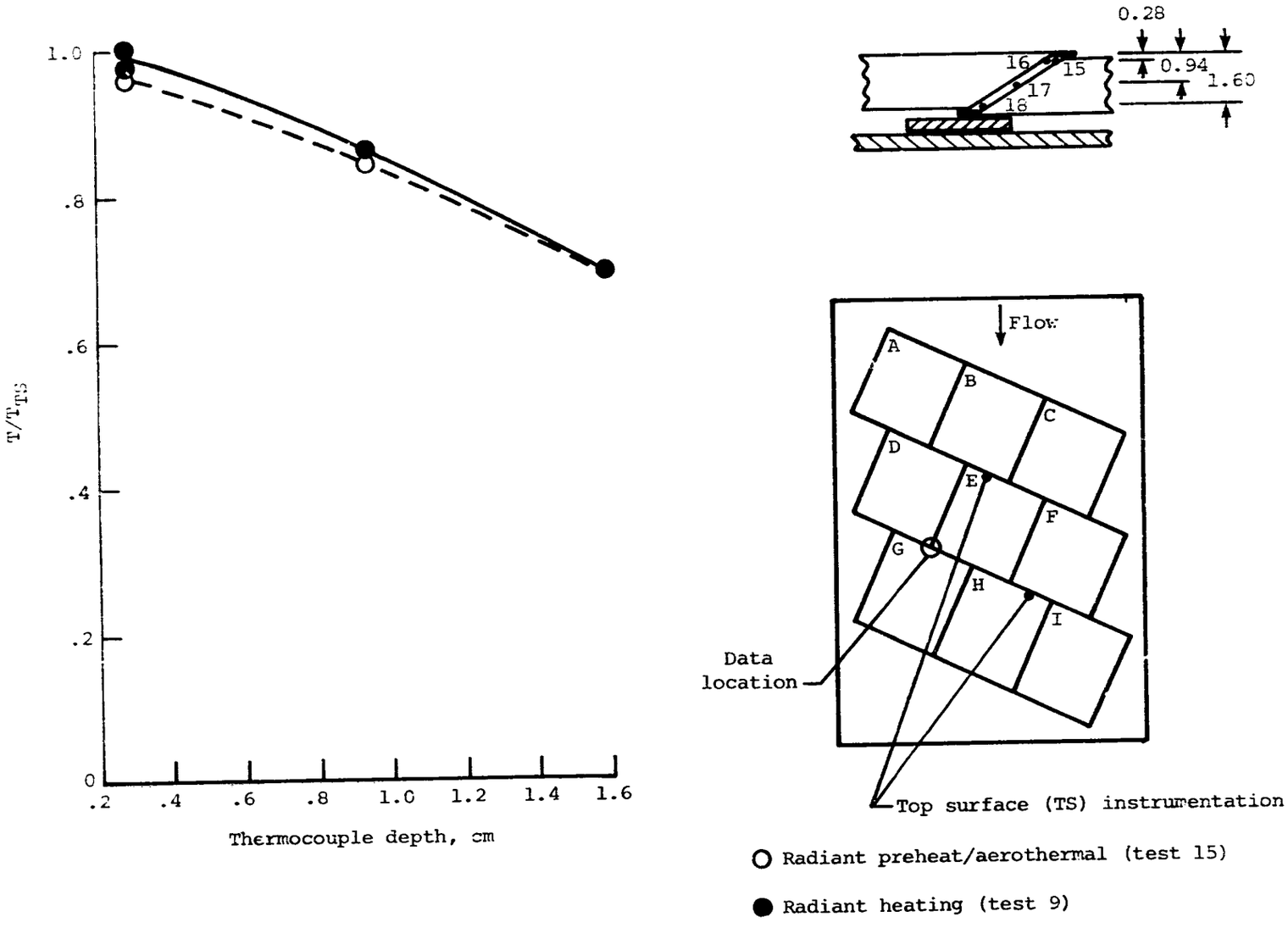


Figure 33.- Heating characteristics in gap. Dimensions are in centimeters.

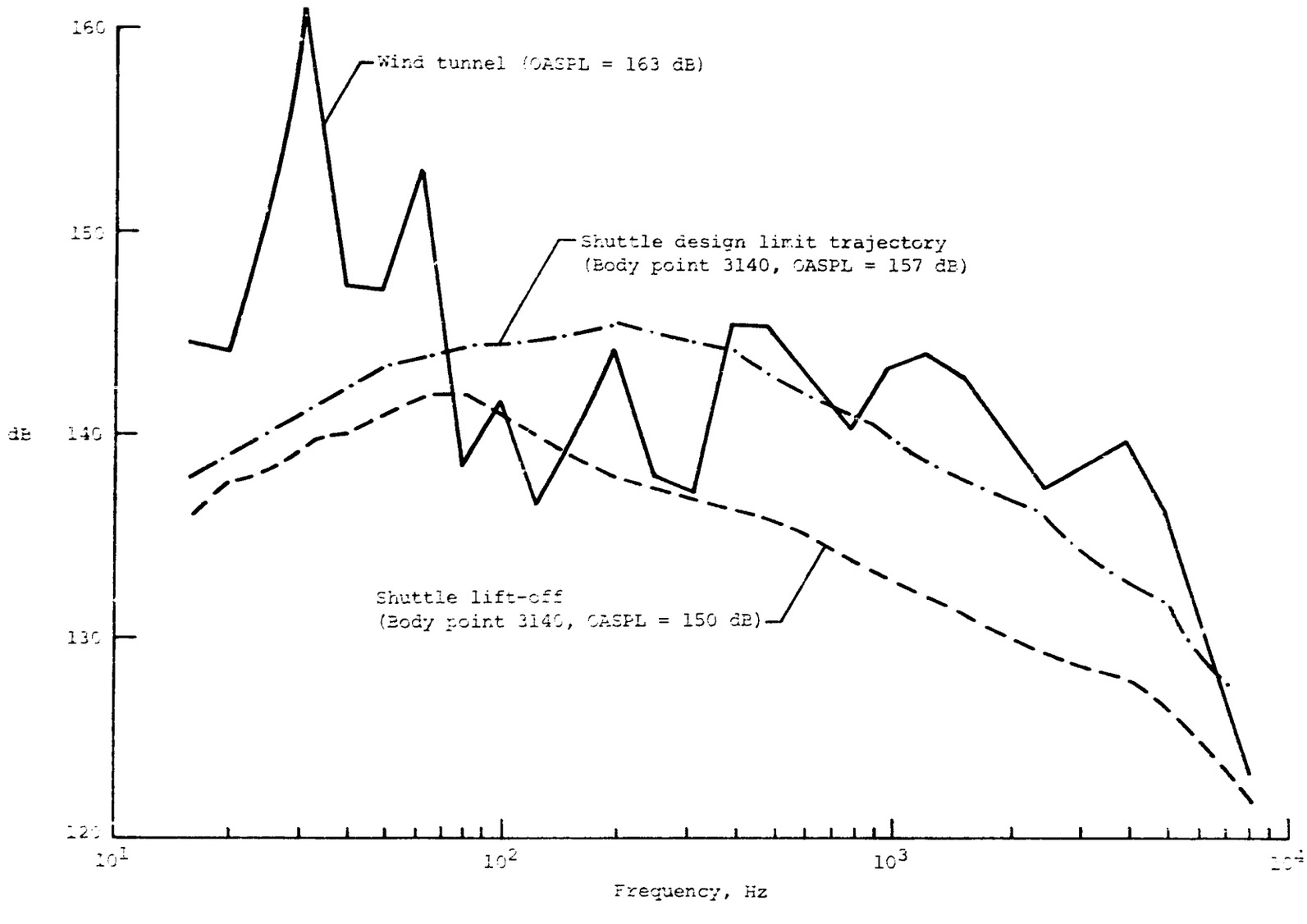


Figure 34.- Acoustic environment (1/3-octave band) in Langley 8' HTST (test 14).